6-2013

Measurement of Skin Friction Drag on Hydrophobic Silica Aerogel Surfaces with Potential Application to Technical Swimsuit Design

Matthew R. Wahl
Union College - Schenectady, NY

Measurement of Skin Friction Drag on Hydrophobic Silica Aerogel Surfaces with Potential Application to Technical Swimsuit Design

By Matt Wahl

****

Submitted in partial fulfillment

of the requirements for

Honors in the Department of Mechanical Engineering

As a student at Union College, I am part of a community that values intellectual effort, curiosity and discovery. I understand that in order to truly claim my educational and academic achievements, I am obligated to act with academic integrity. Therefore, I affirm that I will carry out my academic endeavors with full academic honesty, and I rely on my fellow students to do the same._____

Abstract:

WAHL, MATTHEW Measurement of Skin Friction Drag on Hydrophobic Silica Aerogel Surfaces with Potential Application to Technical Swimsuit Design. Department of Mechanical Engineering, June 2013.

ADVISOR: Dr. Ann M. Anderson

The goal of this project was to fabricate and test a prototype technical swimsuit (low-drag suit worn by swimmers in their most important races) that utilized the hydrophobic properties of silica aerogels. This process involved coating a preexisting suit with aerogel material and completing the build of the newly redesigned water channel at Union College. To evaluate performance of materials, surface drag testing of airfoils coated in aerogel materials was performed using a dynamometer in the water channel. Several additions were made to the water channel in order to reduce variation in drag results. Variation was successfully decreased from 134% to 8.7%.

Results from the aerogel drag testing were compared to similar tests run on airfoils covered in racing suits that are worn by professional swimmers. Drag coefficients ranging from 0.037 to 0.040 were calculated using dynamometer drag readings. Sessile drop tests were performed to measure the contact angle of a drop of water 2 μL on the surface of each material. Contact angles greater than or equal to 135 degrees were found for all items tested. It was found that aerogel coated suits performed comparably to racing suits in drag testing and outperformed racing suits in contact angle testing.

Table of Contents

Table of Contents

Chapter 1: Introduction

1.1 Technical Swimsuits

Technical suits are those worn by elite swimmers in their most important races and therefore must exhibit superior hydrophobic properties. Ideally, these suits will have the ability to physically withstand being submerged in water that is highly chlorinated for extended periods of time.

In the world of technical swimwear, there are three suits generally considered to have the best blend of performance and endurance: the Speedo Fastskin 3, which is made primarily from Lycra and Nylon, the TYR AP12, also made primarily from Lycra and Nylon, and the ARENA Powerskin Carbon Pro, which has Carbon-Fibers embedded in a grid of Polyamide and Elastane. Figure 1 shows the three suits.

Figure 1. The three most popular technical suits. The Speedo FS3 is located on the left (9), the TYR AP12 in the middle (11) and the Arena Powerskin Carbon Pro on the right (2).

The Federation Internationale de Natation (FINA) is the governing body for the world of swimming. In recent years they have passed several legislatures that have limited the possibilities for technical suit design. The two most important of these legislations

essentially state that a suit may not extend below the knees or above the navel for male swimmers, and that all technical suits must be made from 'textile fabrics,' not from a synthetic material. The specific rules pertaining to swimsuit material are reprinted from the FINA guidelines below: (FINA Bureau, 2011).

- Type of material: the material used for swimsuits can be only "Textile Fabric(s)". For the purpose of these rules, this is defined as material consisting of, natural and/or synthetic, individual and non-consolidated yarns used to constitute a fabric by weaving, knitting, and/or braiding.
- Surface treatment of the textile fabric: any material added on to the surface of the textile fabric (e.g. coating, printing, impregnation) shall not close the open mesh structure of the base textile fabric. The treated material shall also comply with all requirements, particularly in regard to thickness, permeability and flexibility. This part of the rule does not apply to logos and labels. This applies to both the manufacturing level and the actual use of the swimsuit.
- Flexibility: the material shall be flexible and soft folding.
- Regular flat material: the material shall be regular and flat. The material shall not form outstanding shapes or structures, such as scales.
- Outside application: No outside application shall be added on the material.
- Thickness: the total thickness of material(s) used shall have a maximum value of 0.8mm. The thickness of layered materials is the total thickness of all layers measured together. It is clarified that this maximum thickness does not apply to seams as far as the seams are functional, and their thickness and width result from their natural functions.

- Buoyancy: the swimsuit shall not have a buoyancy affect above 0.5 Newton, measured after application of vacuum.
- Permeability: material(s) used must have at any point a permeability value of more than 80 liters per square meter per second. Permeability values are measured on materials with a standard multidirectional stretch of 25%. However, measures on material which cannot be significantly stretched will be carried out on unstretched, flattened material. Permeability of layered materials is the permeability of layers measured together.

All suits must be approved by FINA before they are allowed in any type of racing format, and therefore must adhere to the previously stated rules. With these new rules have come new technology, but the ultimate goal of technical suits remains the same. This goal is to help the swimmers move as quickly as they can through the water.

To decrease the amount of water resistance the swimmers face during races, it is necessary to try to eliminate the drag on the swimmer. There are two components that contribute to the total drag as a swimmer travels through the water, pressure (form) drag and viscous (skin) drag. The shape of the suit affects the pressure drag and the material of the suit affects the viscous drag. Most of the suits have the same general shape, maintaining very close proximity to the body, with very few protrusions. There is not much else that can be done in this respect to design, so the focus has shifted to trying to minimize skin drag. The focus of this project is to look at the use of superhydrophobic surfaces to reduce skin drag.

1.2 Superhydrophobic Surfaces

The unique combination of surface chemical hydrophobicity with micron scale surface roughness can cause materials to be superhydrophobic. A typical method that is used to characterize whether or not a material is hydrophobic consists of placing a very small drop of water on the surface of the material and measuring the angle that the tangent of the water droplet makes with the plane on which it is resting on. Figure 2 shows an example of a hydrophobic surface with a water droplet resting on it, as well as the measured contact angle.

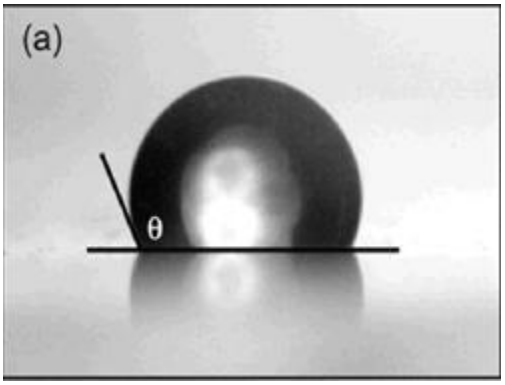

Figure 2. Hydrophobic surface with contact angle shown (Science Direct).

Superhydrophobic materials are characterized by a contact angle greater than 130 degrees. These materials have been known to greatly decrease skin friction (or viscous forces) by creating a layer of air between the material and the water that is flowing around it (Truesdell et al., 2006). This layer of air creates a 'slipping' phenomenon between the surface and the water, which can decrease the amount of friction at the surface. For a swimmer, reducing the amount of force that is required in order to move through the water ultimately allows them to conserve energy, which can then be used in some other fashion, ultimately lowering times and increasing performance.

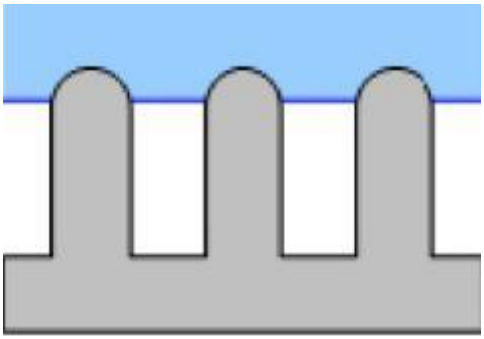

Figure 3. The interface between a micron-scale rough surface and water (Gou et al., 2012).

Two main components contribute to the hydrophobicity of a surface: the chemical makeup and the physical layout. Chemical hydrophobicity

occurs when there are large differences between the chemical structure of the contact surface and water. Because of this, very little interaction occurs between the surface and the water, often even repelling the water. Physical or morphological hydrophobicity is affected by the shape of the contact surface. Surfaces that are the most physically hydrophobic are rough on a very small scale. Ridges due to this roughness create small air pockets between the water and the surface, and decrease the amount of resistance to the flow. Figure 3 shows an example of surface roughness hydrophobicity.

Rodriguez et al. have investigated the use of easily prepared superhydrophobic aerogel surfaces as a method to decrease skin drag. In their research different spindles were coated with aerogels and the amount of torque required for each spindle to rotate in water was measured. This was compared to similar spindles that did not have any coatings, and spindles that had been coated with hydrophilic aerogels. They found that at Reynolds numbers ranging from 2000 to 6000 that there was small but significant drag reduction affect. The superhydrophobic aerogels had 1-5% less drag than the uncoated spindle and 4-9% less drag than the hydrophilic aerogels. For the case of the horizontal spindle it was found that there was as much as a 30% reduction in torque required to rotate the uncoated spindle, and as much as a 35% reduction in torque required to rotate the spindle coated with hydrophilic aerogels, depending on the characteristics of the air trapped underneath the spindle (Rodriguez et al., 2012).

1.3 Aerogels

Silica aerogels can be as much as 99% air by volume, and because of this are known as one of the world's least dense solids. Silica aerogels can be transparent due to their very

low densities. They also have high surface areas and low thermal and electrical conductivities.

Aerogels are typically made using a two-step process. First, a sol-gel polymerization reaction is performed. This process leaves behind a wet gel. The sol-gel solvent is then removed, resulting in a dry, rigid structure. There are two primary methods used to dry the wet gels: silylation methods and supercritical extraction (Carroll and Anderson, 2011). Silica aerogels made using the rapid supercritical extraction (RSCE) method are typically hydrophilic, but can be made hydrophobic by replacing the hydrophilic hydroxyl groups using surface modification.

Anderson et al. (2009) show that hydrophobic silica aerogels can be prepared from a recipe consisting of tetramethoxysilane (TMOS) mixed with methytrimethoxysilane (MTMS). Using this recipe, aerogels have been created with sessile contact angles as high as 155 degrees in a relatively short period of time (7-15 h).

1.4 Project Goals

The goal of this project was to determine if technical swimsuits that are coated with aerogel material can reduce drag on a swimmer, and develop a prototype suit, to be tested and compared to the existing suits that were discussed above. To complete this study, four specific tasks were identified:

1. Complete the construction of the newly redesigned water channel.
2. Characterize the previously discussed technical suits by contact angle and drag measurements.

3. Develop a method to coat suits with aerogels that conforms to FINA requirements for technical suit design, and fabricate a suit using this method.
4. Perform the same characterization tests on the fabricated suit that were performed on the technical suits (see task two).

The rest of this report outlines the steps that undertaken to setup and use the water channel for testing (Chapter 2), the prototype suit fabrication process (Chapter 3), the procedure followed to perform the measurements previously outlined (Chapter 4), and the results of the measurements with discussion (Chapter 5). Additionally, the end of the report contains photographs of the final aerogel coated swimsuit, with a summary of this project and potential related future work (Chapter 6).

Chapter 2: Water Channel Design, Construction and Instrumentation

This section of the report describes the steps undertaken to complete the build of the water channel that was needed in order for drag testing to be performed.

2.1 Background

Prior to the start of this project it was necessary to complete the build of the redesigned water channel. This project was started by Rob Wagner (Union College, 2013) in the summer preceding the fall term of the 2012-2013 academic year. Below I overview the work that he completed, as well as highlight the steps that needed to be taken to complete the channel's fabrication.

2.2 Design

The beginning portion of Wagner's work consisted of evaluating the student-designed water channel that was previously owned by Union College. After thorough assessment, Wagner found that the following changes needed to be incorporated into the new channel's design (Wagner, 2012):

- Incorporate flow conditioning to straighten flow before the test section,
- Use smoother bends in settling tank to prevent onset of turbulence before test section,
- Increase pumping power to allow for a wider test section while maintaining a maximum flow speed of roughly 39 in/s,
- Lengthen the test section and widen the outlet chamber to eliminate backwards flow in the test section,

- Use materials other than wood (such as acrylic or sheet metals) to give the system longevity and to eliminate leakage,
- Incorporate a universal control valve for throttling the water in every pump and controlling flow rate,
- Incorporate a way to monitor the water temperature for experimental purposes and design a system that can more readily dissipate heat,
- Incorporate a way to easily measure the average flow speed in the test section,
- Write a thorough user manual for operating the system.

The majority of these design goals were accomplished. Figure 4 shows the SolidWorks drawing of Wagner's final design, with several of the important components labeled, including the test section, the flow conditioner and the channel inlet. The dimensions of the test section are shown.

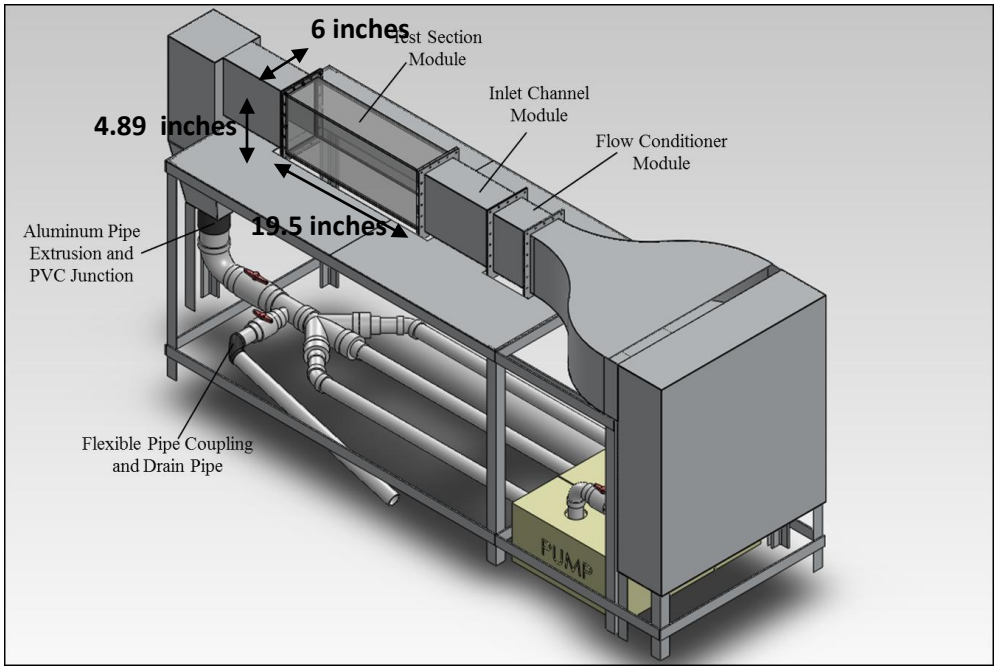

Figure 4. The final design of the water channel, including some important dimensions, is shown. The drawing was done in SolidWorks Education Edition (Wagner 2012).

A copy of Wagner's full report on the redesign of the water channel can be found in Appendix A.

2.2 Water Channel Assembly

At the start of the Fall term 9 items were identified that needed to be done to complete the build of the channel:

1. **PVC Piping:** The majority of the PVC piping components had been purchased, but several still needed to be cut and sized appropriately. All of the PVC piping needed to be dry-fitted and then glued together.
2. **Moving**: The parts of the channel that had been fabricated in the machine shop needed to be moved to their final location in N007 of the Science and Engineering building.
3. **Wiring**: One of the pumps needed to be wired in so that it received power in N007.
4. **Latches:** Latches needed to be attached to the top of the settling tank and the outlet chamber.
5. **Table:** The table that held the flow section needed to be height-adjusted in order to eliminate excess stresses on the metal.
6. **Water:** Upon the completion of all of these things, water needed to be placed into the channel and the entire setup needed to be leak tested, as well as tested to make sure that flow was indeed parallel and laminar as desired.
7. **Flowmeter:** A device for measuring flow velocity needed to be obtained, and a correlation between the openness of the three pump valves and the corresponding flow velocity needed to be created, so that it would be easier for future users to achieve desired test velocities.
8. **Dynamometer Mount:** A mount for the dynamometer that was used for testing the different materials needed to be created.

2.3 Tank Assembly

The sizing and assembly of the PVC piping took four weeks to complete. All of the connections between pieces were measured and appropriate length connection pieces were cut from long tubes. Several additional pieces, including adaptors for the pumps, as well as valves that linked the outlet of the pumps to the settling chamber were purchased. Table 1 shows the different size pieces and quantities that were cut in the machine shop.

Table 1. Lengths and quantities of PVC piping that were cut at the machine shop.

Diameter (inches)	Length (inches)	Quantity
4	4.5	1
3	3.5	2
3	3.25	1
3	3	3
2	42	2
2	40.5	1
2	4.75	3
2	2.5	3
2	2.25	1
2	1.75	2

After all of the pieces were cut, the PVC piping was dry-fitted to make sure that everything was going to fit correctly, and eventually glued together using Oatey brand PVC primer and cement. This process was completed in N007. After all of the PVC piping was in place, water was placed into the channel and several leaks were found.

The most problematic area proved to be the connections between the PVC piping and the pumps (see Figure 5). At these points, a flanged adaptor piece is screwed into the

pump. If this piece is not tightly connected so that it is completely flush, or there is any sort of separation between the flanged adaptor and the pump inlet/outlet, leaking will occur. There are a total of six pump connections. Of these six, three had significant leaks. A process of draining the tank, patching the leaks using Oatey brand epoxy putty, and refilling the tank was repeated until all of the leaks were no longer present. This process took two weeks to complete. Figure 5 shows a picture of one of the pumps that provides the flow in the channel. The epoxy putty was used in order to patch up the leaks that were located on both the inlet (left side of picture) and outlet (right top of picture) of the pump.

Figure 5. One of the three pumps that push water into the settling chamber of the water channel. Both inlet (left) and outlet (top right) had leaks and were patched using the epoxy putty.

Water was loaded into the channel and the pumps were turned on in order to visually inspect the flow. In the test section, the flow appeared to be laminar and parallel,

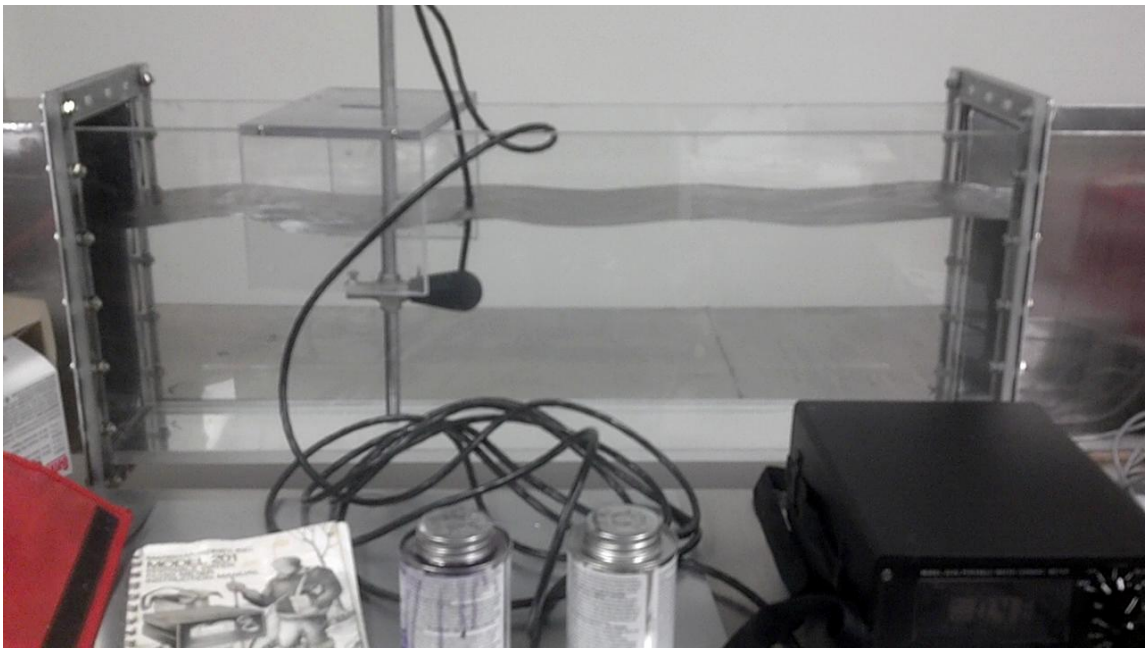

Figure 6. The standing waves present in the first setup of the water channel.

however, undesired standing waves were also present in the test section, as shown in Figure 6. Upon further examination of the entire flow channel, it was found that the cause of these standing waves was the flow straightener in the flow conditioner module (see Figure 4). As water attempted to flow into the straightener, a pressure buildup caused a significantly higher water level at the inlet to the straightener than the outlet, causing different flow velocities at the top and the bottom of the straws that were being used to straighten the flow. Figure 6 shows a sketch of this phenomenon.

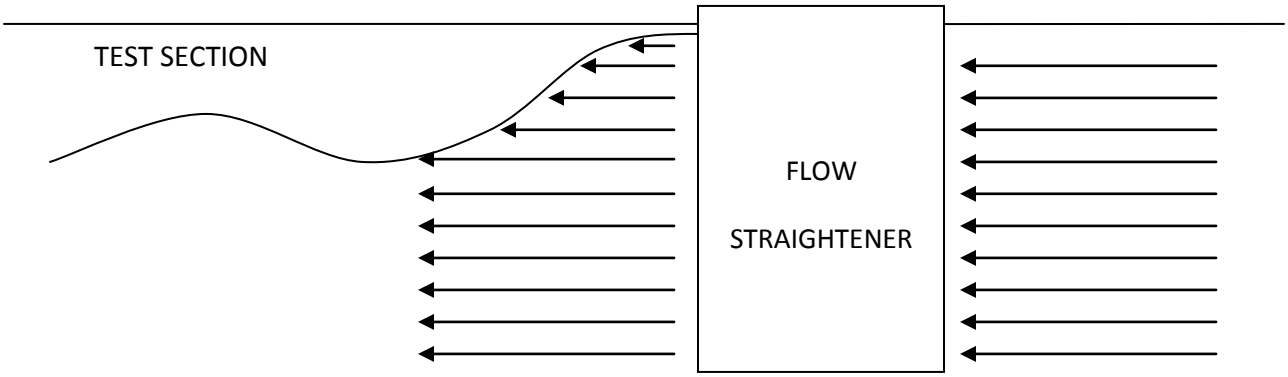

Figure 7. Sketch showing the origin of the standing waves in the test section.

To fix this problem, the flow straightener was moved. Prior to relocation the straightener was 'upstream' of the test section. It was moved to immediately downstream of the test section. This helped to steady the flow ahead. Although the straws could no longer provide the same effect as they originally had been designed to do, the difference in position did not cause any significant problems with the flow, and solved the issue of the standing waves.

2.4 Velocity Meters

To use the channel, we need to be able to measure flow velocity. It was decided that a device be obtained that could be easily used and mounted to the water channel that measured the test section's flow velocity. There are several different kinds of water velocity meters. Different techniques of varying complexity are used to measure how quickly water is flowing. Two types of devices were investigated as potential purchased additions to the channel--impeller based flowmeters and magnetic flowmeters.

The simplest types of velocity meters involve impellers that rotate based on how quickly the water is traveling through them. The pressure force exerted by the water onto the blades of the impeller cause rotations, and the number of rotations in a given period of

time is linearly related to the flowrate of the water. More expensive flowmeters use magnetic sensors to effectively measure the water's speed. These devices work by utilizing Faraday's Law of Electromagnetic Induction. A magnetic field is generated and as the water flows through the magnetic field the ions in the water cause a small amount of voltage to be generated, which is monitored by sensors mounted on the outside of the pipe's walls. With higher levels of flow, greater voltages are measured, and a correlation is used to obtain the water's velocity.

Because of its very expensive price, it was decided that a magnetic flowmeter was too costly to be purchased for the channel. While searching for an appropriately priced impeller flowmeter, several viable options were found that were intended to be used as stream velocity meters. Typically these items are used by Geologists or Environmental Scientists in order to gauge the velocity of a stream in the wilderness, but due to their ease of use and relative availability, they were considered appropriate for the task of monitoring flow velocity in the test section of the water channel.

There are several different types of stream flowmeters. The cheapest and least accurate style utilizes the impeller approach. More expensive models monitor the flow of the water by relating the pressure measured at different positions of the tip of a bulb-shaped mount that is placed in the water. Upon further inspection it was found to be unwise to purchase a stream flowmeter as most models were too expensive to be primarily used as a mount in the water channel. Union College's Geology department was contacted, and a Marsh-McBirney Inc. Model 201 portable water flowmeter was provided for extended use. This flowmeter, shown in Figure 8, can read velocity values from 0.00 to 6.10 meters per second with an accuracy of ±2%.

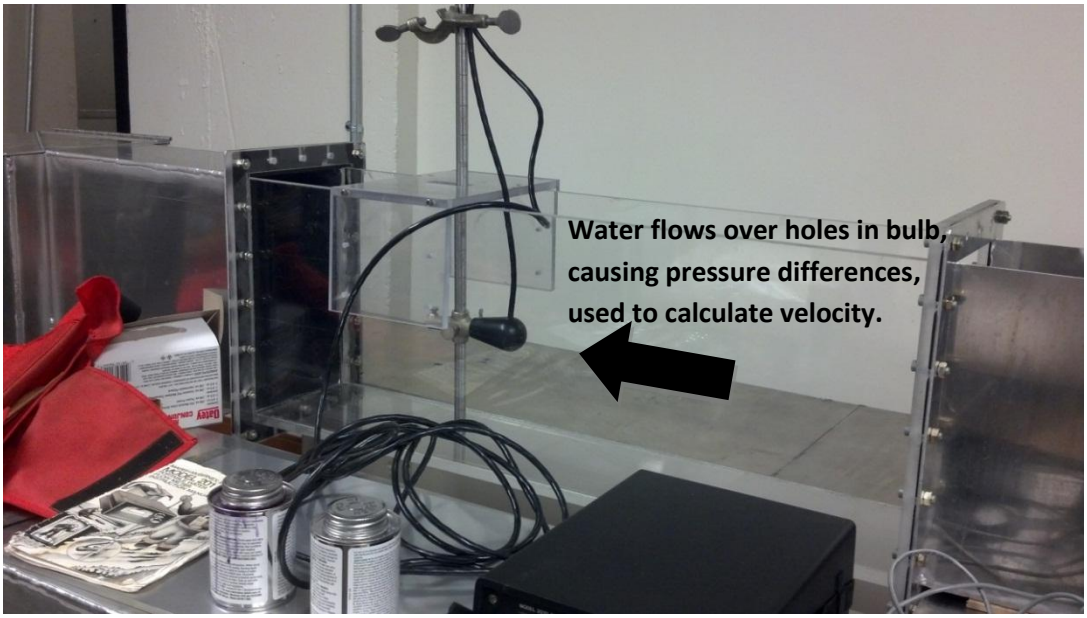

Figure 8. The flowmeter used to measure water velocity in the channel, which was borrowed from the Geology department.

2.5 Water Channel Calibration

Now that the flow velocity could be accurately measured, it was possible to calibrate the water channel so that a relationship between the state of each of the three valves controlling the pumps and the flow velocity could be developed. The calibration was performed with the thought that each of the valves could be placed in one of three positions: open (90°), half-open (45°) or closed (0°). This created a total of 27 different possible combinations of valve positions. Table 2 shows the calibration data.

According to the calibration data, the maximum flow speed that is possible in the test section is 0.74 meters per second. Using just the combination of these three positions it is possible to obtain a broad range of values for flow velocity in the test section. The range of Reynolds Numbers that can be obtained in the test section for flow over a 12 inch flat plate is 30,400 to 224,700 (see Appendix B for information on the calculation). Using a similar process the range of Reynolds Numbers that can be obtained in the test section for

flow around a 2 inch diameter sphere is 5,060 to 37,400. These ranges imply that all testing will be done in flow that is laminar.

Table 2. Calibration data for the relationship between the valve positions and the flow in the test section of the water channel. Red boxes correspond to closed valves, yellow to half-open valves, and green to fully open valves.

Angle Pump 1 (°)	Angle Pump 2 (°)	Angle Pump 3 (°)	Velocity (m/s)
0	0	0	0.00
0	45	0	0.10
0	0	45	0.11
45	0	0	0.12
0	90	0	0.20
0	0	90	0.20
90	0	0	0.20
45	45	0	0.26
45	0	45	0.27
0	45	45	0.28
0	90	45	0.34
90	0	45	0.34
0	45	90	0.36
90	45	0	0.37
45	0	90	0.37
45	90	0	0.38
0	90	90	0.43
90	90	0	0.43
90	0	90	0.44
45	45	45	0.47
45	45	90	0.58
90	45	45	0.58
45	90	45	0.59
90	90	45	0.60
45	90	90	0.62
90	45	90	0.62
90	90	90	0.74

2.6 Dynamometer

An Engineering Laboratory Design dynamometer is used to measure the drag force on the different materials as they are placed in the water channel. Inside the dynamometer there is a linear variable differential transformer. A force is applied to the dynamometer input, and this torque creates a small amount of linear displacement. The linear displacement causes a small amount of induced voltage inside the device. This voltage is read by a data acquisition device. Instantaneous voltages are monitored over a long period of time and an average is taken to obtain the mean force that is present on the dynamometer. The dynamometer is capable of reading drag up to 8 pounds (35.58 N, 3.62 kg). A schematic of the dynamometer can be seen in Figure 9. A picture of the device can be seen in Figure 10.

Before testing was completed it was necessary to calibrate the dynamometer. Because the value of the drag readings that were going to be obtained was so small, the 'gain' on the dynamometer was increased to its maximum possible level. A calibration was then performed by connecting the dynamometer to an MCDAQ USB2498 data acquisition system. The DAQ system records voltages that are outputted by the dynamometer. By hanging weights of varying values on the end of the dynamometer and recording the amount of voltage that is read, it is possible to find a correlation between the force on the dynamometer and the voltage that is outputted. Figure 11 shows the magnitude of the weights hung and the voltages read. The calibration equation is represented by Equation 1.

$$Mass(g) = 14.64 * Voltage - 0.7172 \quad (1)$$

In order to use the calibration equation, one must simply take readings using the dynamometer and the DAQ system and take the average voltage that is measured. This voltage can be substituted into Equation 1 and then a mass can be obtained. Using this mass value and Newton's 2nd law it is possible to calculate the drag force.

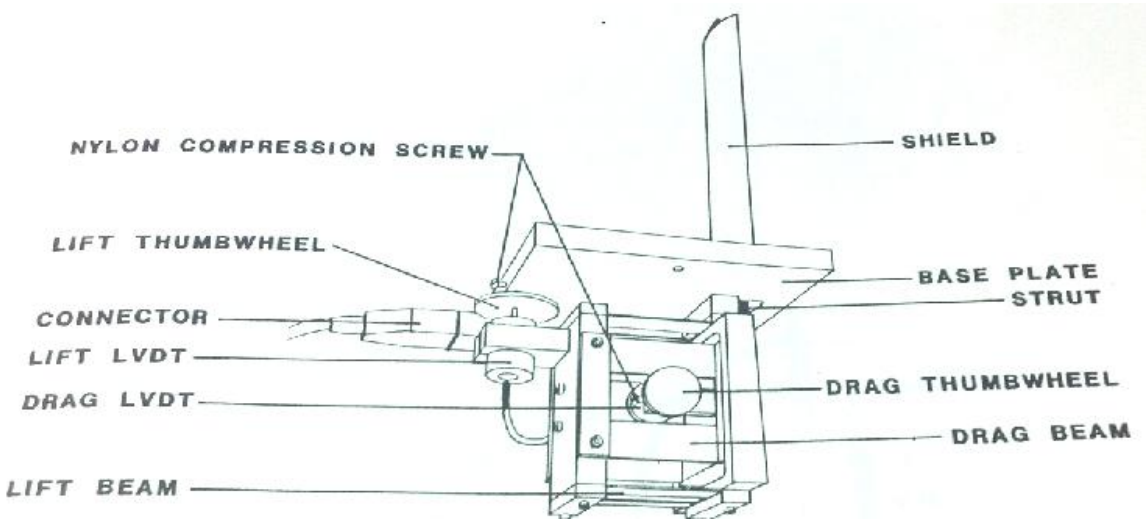

Figure 9. Dynamometer Schematic, taken from the Engineering Laboratory Design handbook.

Figure10. Picture of the dynamometer.

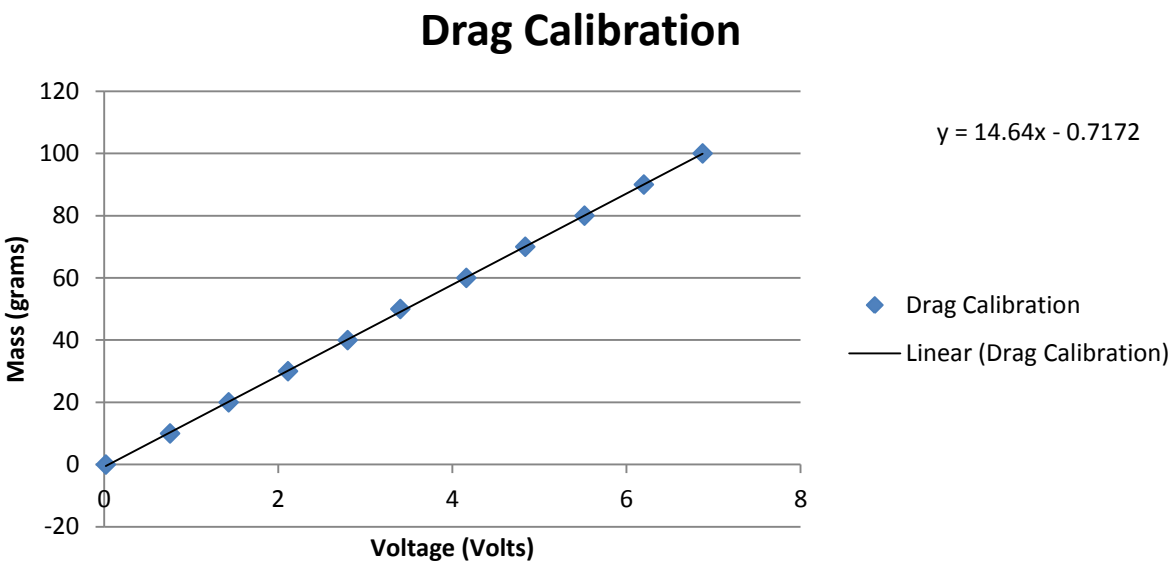

Figure 11. The calibration data for the dynamometer. The y-axis represents the mass of each of the weights that was hung on the dynamometer and the x-axis shows the voltages that were read. The calibration equation is located to the right of the graph.

A method of mounting the dynamometer on top of the test section needed to be devised. A simple design that slides in and rests on top of the test section was created in SolidWorks Education Edition and can be seen in Figure 12.

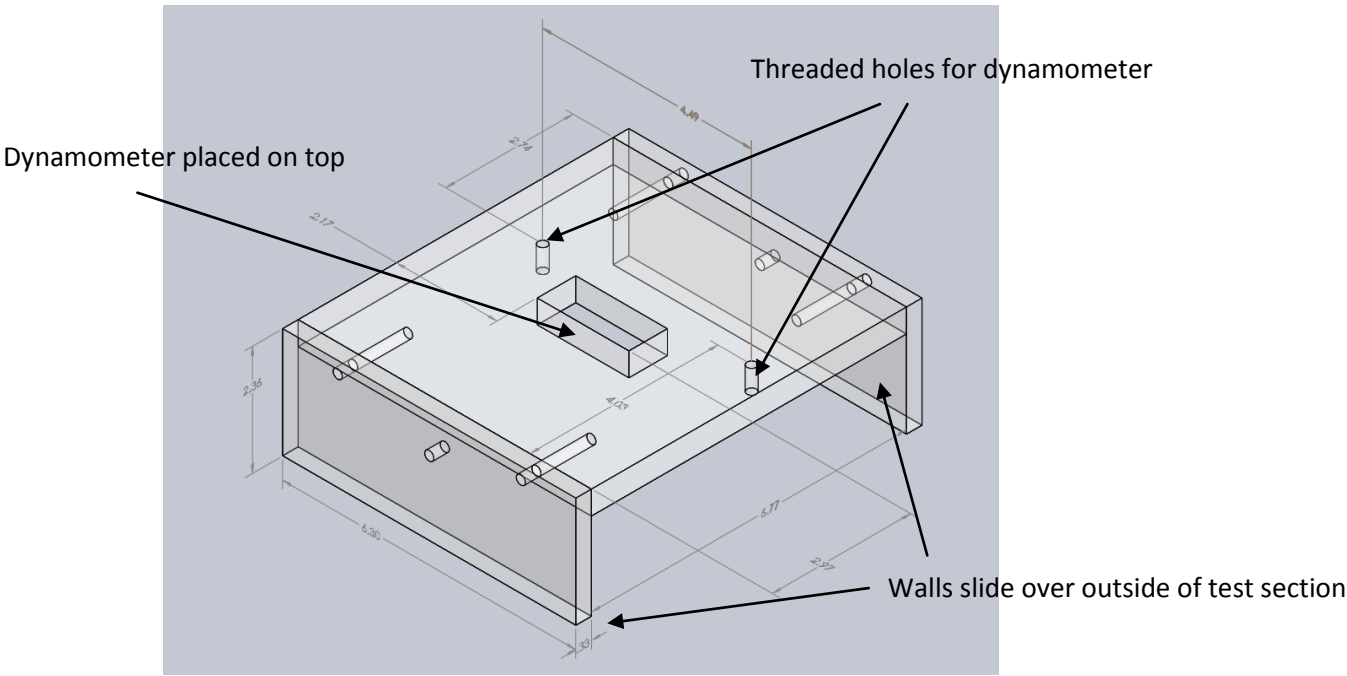

Figure 12. Designed mount for the dynamometer. Drawings performed in SolidWorks Education Edition. All units are in inches. All holes are 0.2 inches in diameter.

One of the most important parts of the mount is the top segment. The design focused on the ability to easily place and remove the dynamometer. Threaded holes were created based on the existing dynamometer, which has places in which it can be bolted in to any existing test chamber. The two individual holes that are located on the outside wall of the mount are to be used as 'clamps' if the design begins to move too much without the clamps then bolts will be placed into them and tightened on the outside of the test section until the mount is completely stationary.

2.7 Drag Testing Design 1

Once a mount was designed it was necessary to craft an item that the different fabrics could be tested on. It was decided that in order to eliminate any flow separation, an airfoil would be best suited for this purpose, and one was designed in SolidWorks Education Edition. The airfoil was designed to match NACA0012 specifications. The cross section of this airfoil can be seen in Figure 13.

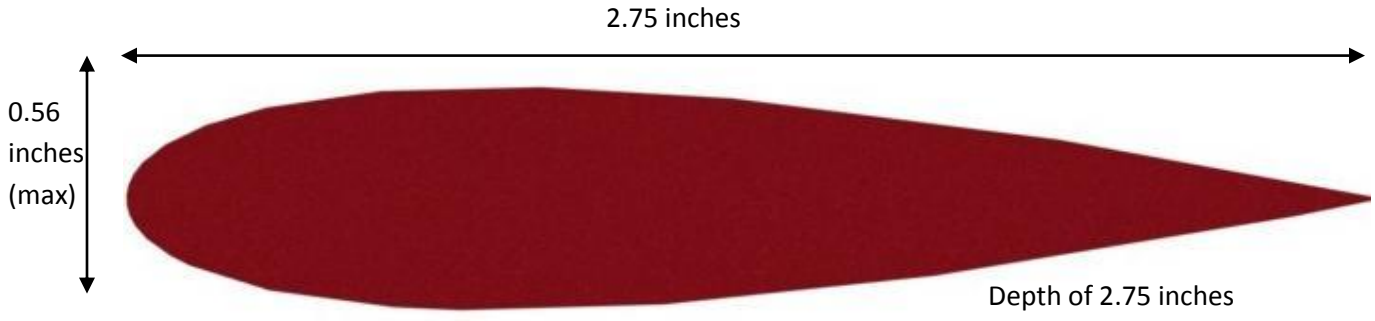

Figure 13. Cross section of NACA 0012 airfoil designed in SolidWorks Education Edition, with dimensions.

Eight of these airfoils were manufactured using a 3-dimensional printer. Originally it was planned that for testing, five of the airfoils will be covered with suits, three of the

airfoils will be coated in aerogels, and one airfoil will be used as a base standard for the others to be compared to.

A total of eight pieces were fabricated to connect the airfoils to the dynamometer. Each individual piece was glued onto the top of an airfoil, and connects to the input of the dynamometer via screw (see Figure 9). Figure 14 shows this connector piece.

A design flaw was found in the dynamometer mount (Figure 12). As water flows over the airfoil, it will also hit the front of the connector piece (Figure 14). The mount was redesigned with the addition of a small aluminum 'blocker' in front of where the connector piece will be hit by the flow. If this piece was not added, a significant amount of additional unwanted drag force would be measured by the dynamometer. This blocker piece will cause a significant reduction in the pressure drag from the water that is incoming on the connector (above the airfoil) to be transmitted to the dynamometer. The redesigned dynamometer mount can be seen in Figure 15, placed on top of the test section of the water channel.

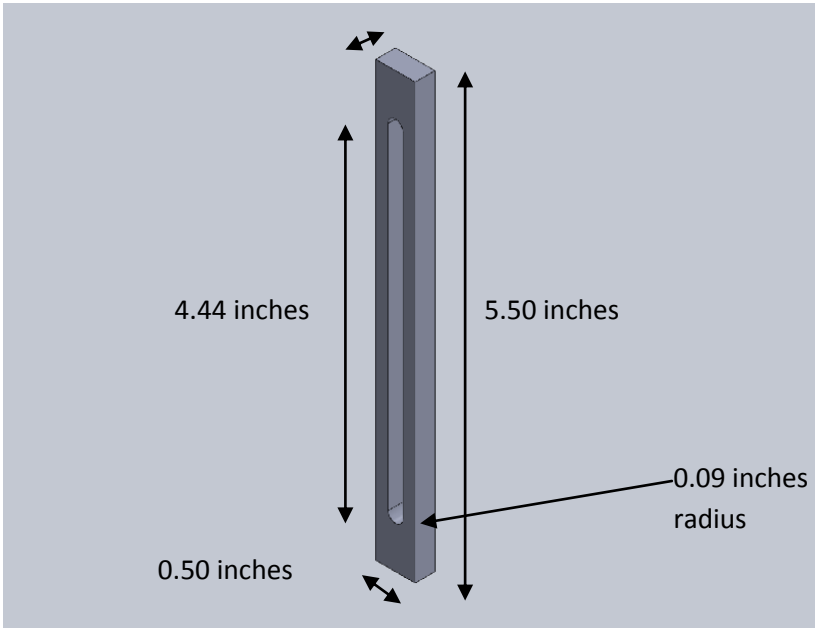

Figure 14. Connection piece glued to the airfoils that screws into the dynamometer. Used in order to take force readings on airfoils.

Figure 15. The dynamometer mount with the blocker added.

As an accuracy test, the uncoated airfoil was placed inside of the water channel and force measurements were read. Table 3 shows the average voltage read by the DAQ system using this airfoil with standard deviation.

Table 3. Voltage data obtained from the first airfoil using the DAQ system. Uncertainties are very high.

Number of Pumps	Flow Speed	Average Voltage	Std. Dev Voltage	%Std Dev Vltg
1	0.20	0.0273	0.1355	496.3
2	0.43	0.1153	0.1549	134.3
3	0.74	0.6194	0.2036	32.9

When examining the data in Table 3, it is apparent that the standard deviation in each of the voltages, which can be used to gauge the consistency of the measurements, was very large. These variations in measurement come from instability in the flow and are undesirable. To combat these large standard deviations, the testing design was revised.

2.8 Drag Testing Design 2

In an effort to lower the large amounts of variation that were associated with the original testing procedure, a second testing process was developed. The strategy involved in doing this revolved around two primary concepts; increasing the value of the drag readings on the dynamometer (thus making voltage variations read by the DAQ a smaller percentage of the average reading), and increasing the uniformity of the flow inside of the test section of the water channel.

The most obvious (and easiest) way to increase the magnitude of the drag force is to simply make the size of the airfoils larger. This was done by gluing together several of the pre-existing airfoils to a make a new test piece. Several different size combinations were created, but it was found that the best option was created by gluing together 3.5 of the airfoils vertically. This new test piece can be seen in Figure 16. The visible glue was removed by sanding before testing began.

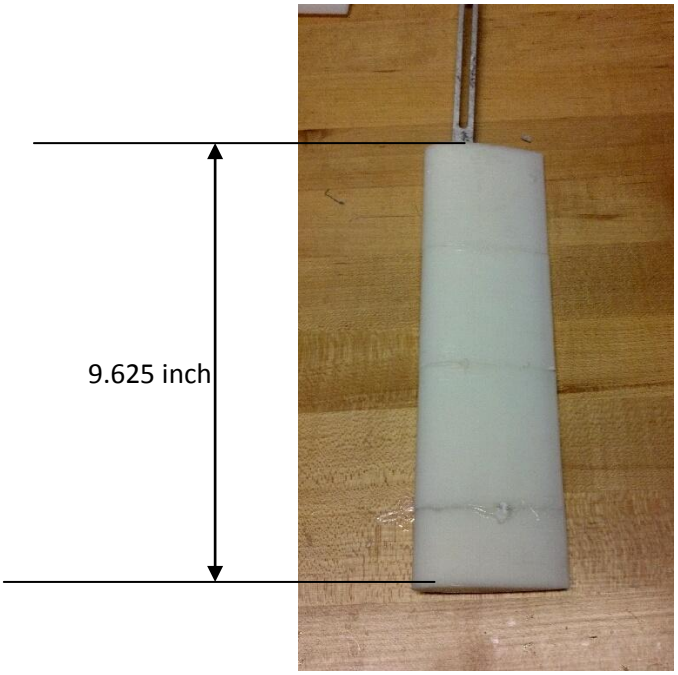

Figure 16. The new airfoil that will be inserted into the test sections for additional testing. This airfoil is made by gluing together 3.5 of the original airfoils that were produced.

2.9 Flow Conditioning

The problem of creating more uniform flow in the test section was not as easy to solve. Research was performed and it was found that often grated metal pieces are inserted as flow conditioners into water channels to make the flow as stable as possible. It was hypothesized that creating a piece in the machine shop and inserting this into the flow would provide for significant flow conditioning. Figure 17 shows the piece that was designed in SolidWorks Education Edition. The piece was designed so that it was the same size as the water channel, and would therefore slide directly into the area before the test section (see Figure 4).

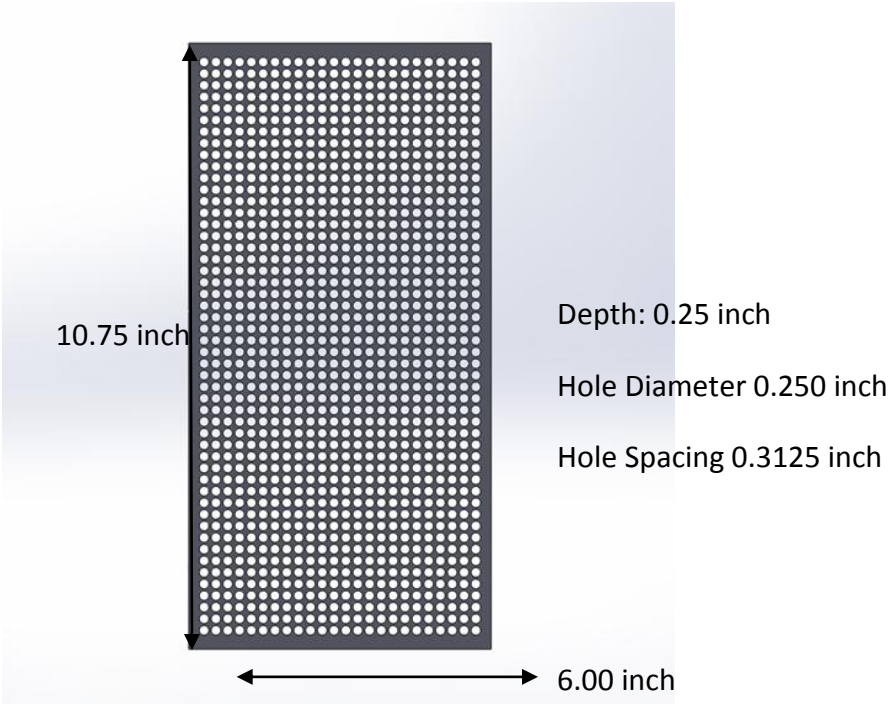

Figure 17: The dimensioned flow conditioning piece developed for the water channel.

The feasibility of the design was discussed with Paul Tompkins in the machine shop and it was decided that although the piece might perform well, it would require far too much time and effort to be machined. Alternatives were discussed and it was decided that the best course of action would be to purchase perforated plates from McMaster Carr.

A perforated plate with 0.156” diameter holes, 0.188” hole spacing, and 63% open space (item number 9255T62) was purchased from McMaster Carr. This large piece was cut into thirteen 6.0 inch by 10.75 inch squares. Figure 18 shows an example of one of the cut pieces. Accuracy tests were once again performed using the DAQ with as many as seventeen squares inserted into the flow, with the water traveling at different speeds. Table 5 shows the full breakdown of tests, with descriptions, average measured voltages, standard deviations, and percent uncertainties. Figure 19 shows the area before the test section with these pieces inserted into it.

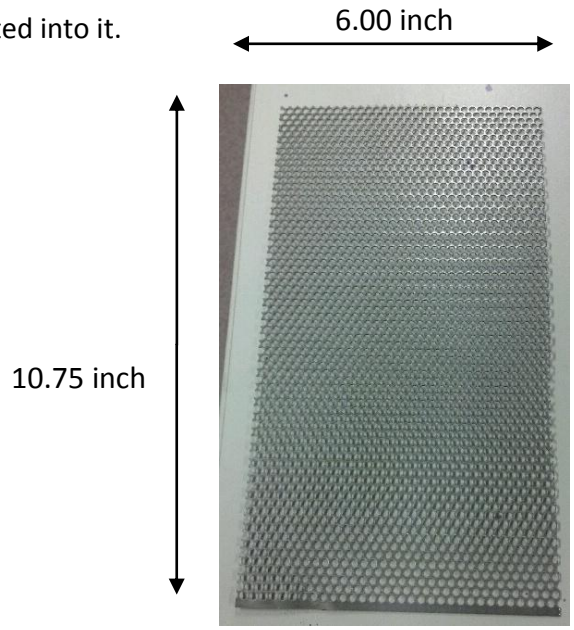

Figure 18. Cut and dimensioned piece that will be inserted into the area in front of the test section. Piece was crafted by cutting down a larger square from McMaster Carr.

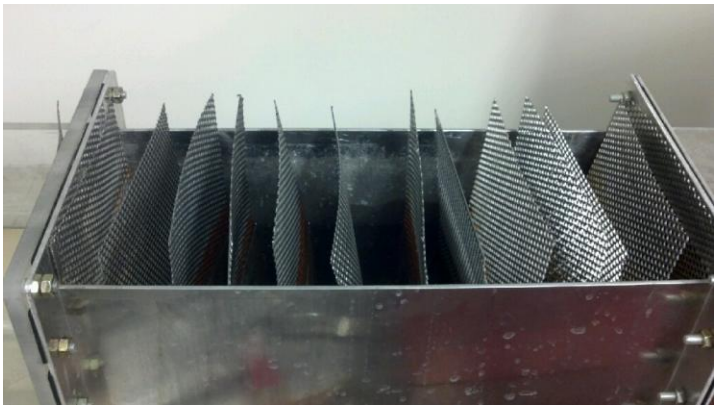

Figure 19. The inserted cut squares into the water channel in order to provide flow conditioning for the test section. A maximum of 17 total pieces were inserted. Shown with 13 pieces inserted.

Table 5. Data for all of the tests run in order to attempt to lower uncertainty. Percent uncertainty is color coded in order to show quality of data.

# of Pumps	Flow Speed	Airfoil	Condition	Avg Voltage	Std Dev Voltage	%Std Dev Vltg
1	0.18	Original	0 gratings	0.1447	0.1634	113.0
1	0.20	Original	1 grating-front	0.0489	0.2221	453.9
1	0.20	Original	1 grating-back	0.5990	0.1810	302.1
1	0.19	Original	2 gratings	0.0550	0.2962	538.7
1	0.21	Original	7 gratings	0.0805	0.2585	321.0
2	0.40	Original	0 gratings	0.3930	0.2446	62.2
2	0.42	Original	1 grating-front	0.3131	0.2526	80.7
2	0.42	Original	1 grating-back	0.3387	0.2194	64.8
2	0.43	Original	2 gratings	0.3575	0.3531	98.8
2	0.60	Large	5 gratings	0.9149	0.1251	13.7
2	0.55	Original	7 gratings	0.2872	0.2047	71.3
2	0.58	Large	7 gratings	0.9011	0.0781	8.7
2	0.55	Large	9 gratings	0.7838	0.1240	15.8
2	0.49	Large	10 gratings	0.7912	0.1496	18.9
2	0.50	Large	12 gratings	0.7662	0.1574	20.5
2	0.53	Large	14 gratings	0.8381	0.1436	17.1
2	0.51	Large	17 gratings	0.7817	0.2547	32.6
3	0.67	Original	0 gratings	0.8497	0.3021	35.6
3	0.73	Original	1 grating-front	0.8142	0.2710	33.3
3	0.80	Original	1 grating-back	0.9311	0.2824	30.3
3	0.79	Original	2 gratings	0.9033	0.2386	26.4
3	0.78	Original	3 gratings	0.6127	0.3354	54.7

It was found that the uncertainty was as low as 8.8% (which is an acceptable level) when 7 of the cut squares were inserted into the water channel with the new larger airfoil.

Chapter 3: Suit Fabrication

This section of the report describes the fabrication of the prototype aerogel suit, or Aerosuit, as it is later referred.

3.1 Suit Fabrication Background

Three different methods were designed to create a prototype suit. Method number one involved purchasing thin yarn and coating it with aerogels, then attempting to knit the fabric into a small, testable piece (using knitting needles). Method number two once again involved purchasing thin yarn and coating it with aerogels, but instead an attempt was made to weave the yarn together using a homemade 'loom.' Both of these methods adhere completely to the standards set forth by FINA (see Introduction-Technical Swimsuits). Method number three consisted of taking a preexisting suit (one that had been used several times and no longer had any hydrophobic properties) and using a spray-on adhesive to coat it with aerogels. The third method violates FINA standards, but ultimately was the only viable option.

3.2 Coating Process

Size 10, 7 gauge knitting thread was purchased from a local fabric store. A setup was created to coat a portion of the thread in aerogels. Roughly 30 meters of the thread was separated from the spool and set aside. Two large nails were nailed into a piece of plywood roughly 2 feet apart. The 30 meters of yarn that had been set aside earlier was wrapped around the two nails. A schematic of the coating situation can be seen in Figure 19.

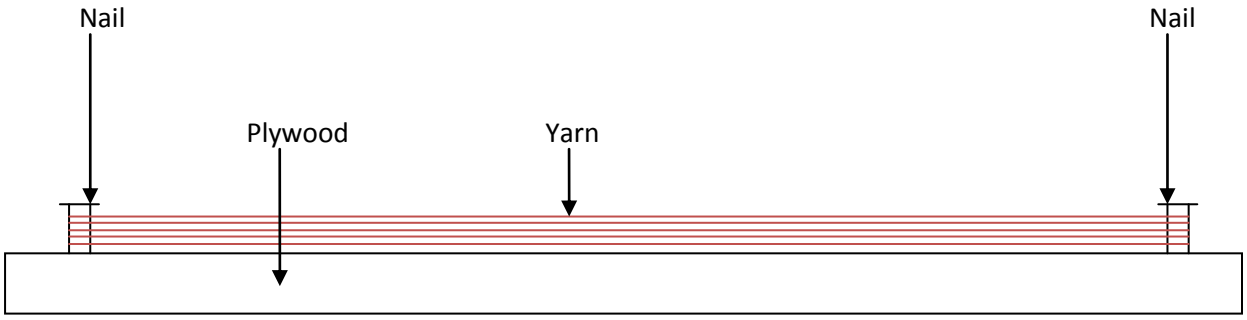

Figure 19. The setup used to coat the yarn with aerogels (not drawn to scale).

After the yarn was wrapped around the two nails, a large amount of aerogels were crushed by hand inside of a large beaker with a removable cap. This beaker was set aside for later use. An adhesive spray was sprayed on the yarn, with focus on the entire length of yarn getting some adhesive on it. Immediately after the adhesive was applied, before it was allowed to dry, the yarn was removed from the setup and placed inside of the large beaker and the cap was placed on the beaker. The beaker was then shaken aggressively for several minutes, in an attempt to try and get the aerogels to stick to the yarn. The yarn was then removed from the beaker and spooled around a section of PVC pipe in order to let dry. Figure 20 shows the spooled yarn.

Figure 20. The spooled yarn that has been coated with aerogels. Note the slight discoloration (white tint) due to the aerogel material.

3.3 Method One-Knitting

The coated yarn was supplied to a knitting expert, who attempted to create a test swatch using the stockinette stitch pattern. It was found that the yarn was significantly too sticky and more than a few stitches could not be made.

3.4 Method Two-Loom

A loom was created using plywood and size ½ x 19 steel wire brads. In order to do this, a square 10 cm on each side was drawn out on the piece of plywood. A mark was made every 3 mm throughout the entire perimeter of the square using a marker. A wire brad was nailed into every one of the marked position. 268 total wire brads were used. Figure 21 shows the final product.

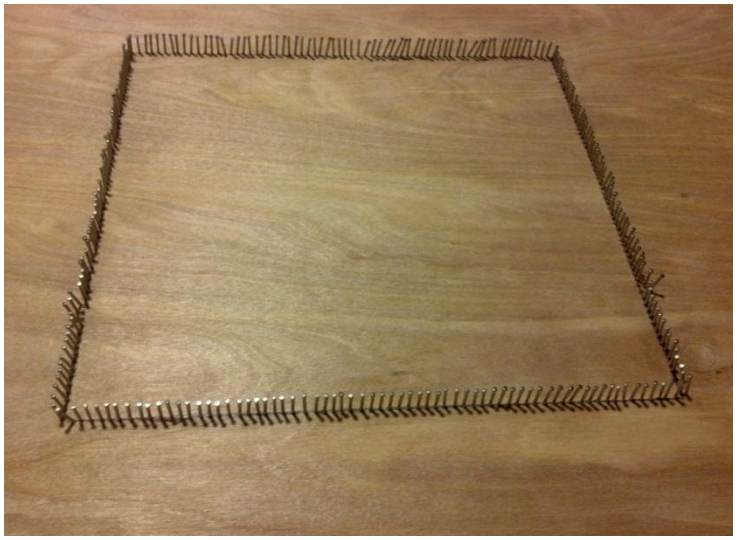

Figure 21. The final product 'loom' that was created.

In theory the yarn could be wrapped around the wire brads in repeated fashion in alternate directions, allowing for a weave to be created. When this method was put into practice with the uncoated yarn, no problems occurred. However, when the coated yarn was used in the 'loom,' the same problem occurred as the knitting. The yarn was ultimately

too sticky to get into a tight weave pattern. Figure 22 shows the attempt to use the loom when this was realized.

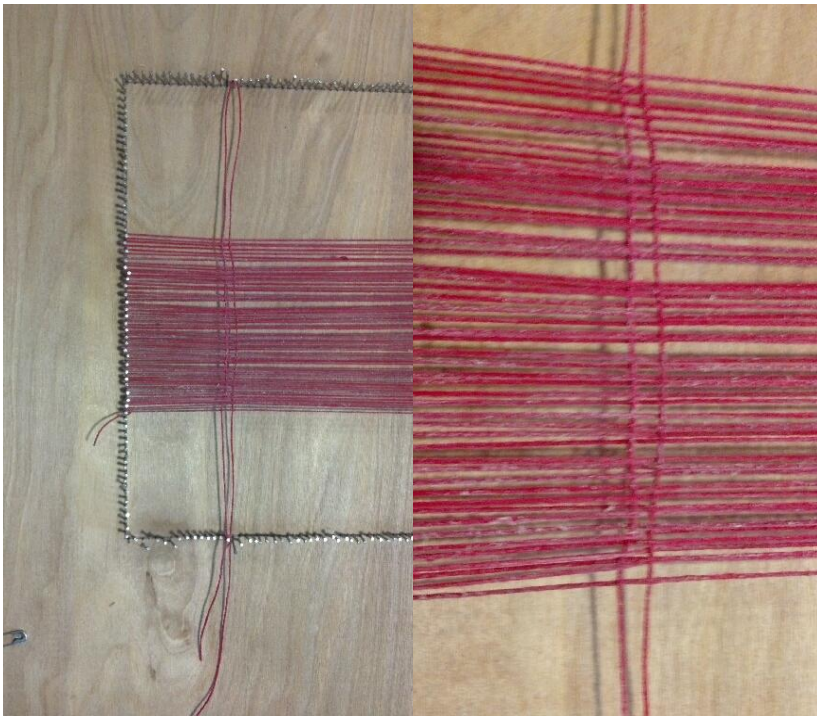

Figure 22. The attempt to use the loom to weave together the coated yarn. The yarn was too sticky to get a tight weave. The image on the right shows a close-up of the yarn. The image on the left shows the yarn inside of the 'loom.'

3.5 Method Three-Preexisting Suit

Due to the struggles faced when trying to weave together yarn that has been coated first, a different method was applied. Instead of coating and then weaving, a preexisting suit was coated with the aerogels. This method violates FINA standards for suit fabrication, as it closes the open mesh structure of the base textile fabric and is an outside application to the original fabric. For the purpose of this study this was deemed both necessary and acceptable. The suit provided a prototype that could be used for proof of concept experiments.

A two year old Speedo LZR pro jammer was used as the starting point for this method. The simple strategy of applying a small portion of the outside of the suit with spray

on adhesive and then placing ground up aerogels on top of the adhesive before it was allowed to dry was used. This proved to be a very effective method for coating, although very time consuming. The finished product can be seen in Figure 23.

Figure 23. The finished aerogel suit.

When viewing the aerogel suit there are some obvious portions where there are light spots. These lighter areas are places where there were thicker applications of adhesive as the aerogels were sprinkled onto the suit. The extra glue caused the aerogels to build up and no longer give a transparent appearance.

One important thing to note about the suit that was used is the age and large amount of use that it had received. Although the suit was at one point exceptionally hydrophobic, it had been worn in many races prior to being coated. This has caused a significant decline in the properties and performance of the suit. Because of this, there was no concern that the suits old hydrophobic properties would positively skew the data for the aerogels.

3.6 Aerogels

All of the aerogels that were used to cover the suit shown in Figure 23 were created at Union College using the rapid supercritical extraction method. The two main components of the aerogels used for testing are MTMS (methyltrimethoxysilane) and TMOS (tetramethylorthosilicate). Both of these chemicals are organic and have very complex molecular structures.

The process to create the aerogels used begins with the fabrication of regular silica aerogels (100% TMOS). Anderson et al. state that this process consists of some of the Si-OCH_3(Si-OR) groups being hydrolyzed Si-OH, which then undergo condensation reactions, resulting in a large Si-O-Si network. After gelation, some of the Si-OR and Si-OH groups still remain unreacted, and those groups are prone to adsorption of water, which makes the resulting aerogel hydrophilic.

Hydrophobic aerogels are prepared in a similar manner, except the solvent consist of TMOS and MTMS. The TMOS undergoes a hydrolysis reaction, and when enough of the TMOS has been hydrolyzed, the rate of MTMS hydrolysis increases, which results in methyl groups (CH_3) bonded to silicon, rather than the hydroxyl groups. The Si-R groups are hydrolytically stable, so the resulting aerogel is hydrophobic (Rodriguez et al. 2012).

By varying the amounts of TMOS and MTMS present in the aerogel, it is possible to change the physical properties of the compound. Aerogels with higher percents of MTMS exhibit the strongest hydrophobic properties. For this reason, 50% and 75% MTMS aerogels were tested in this study. The suit shown in Figure 23 is coated with 50% MTMS aerogel material.

Chapter 4: Experiments (Contact Angle and Drag Testing)

Two primary tests were performed on the different materials: contact angle testing and skin friction testing using a dynamometer. These tests are outlined below.

4.1 Contact Angle Testing Procedure

Sessile drop tests were performed using a Kruss DSA100 contact angle instrument for five different materials. Tests were done on microscope slides that had the superhydrophobic materials attached to them via double-sided tape. Materials tested included the Speedo LZR Elite, A3 Stealth, TYR AP12, 50% MTMS aerogels, and 75% MTMS aerogels. Drop sizes of 2 µL were used for all tests, and 30 drops were measured on each surface. Average and standard deviation values were calculated for each surface.

4.2 Skin Friction Drag Testing Procedure

In order to test the skin friction of each of the different materials, the airfoil discussed in section 2.8 was covered using two-sided tape. The best method to do this involved cutting out a square of double sided tape that was 5.5 inches by 8.5 inches (roughly the surface area of the airfoil that is tested) and sticking this to a portion of the suit (while making

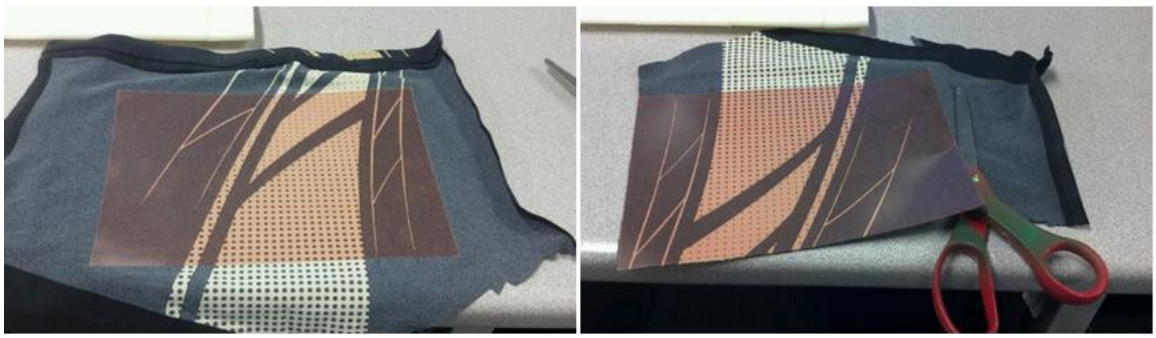

Figure 24. Left: the two-sided tape stuck on to the inside of the suit. Right: the excess suit being cut off from the outside of the tape.

sure the suit had no folds or ripples in it). The suit was then cut to match the size of the portion of tape. This square of material was then folded over the airfoil, covering the side that the water was incident on primarily. Figure 24 shows the steps involved in this procedure. Figure 25 shows the final products for all four suits. It is important to note that the cross-sectional area of the airfoil changes when it is covered with each suit. The increase in cross-sectional area causes an increase in planform area for the airfoil, which is used in the calculation of the drag coefficient. This effect is discussed in more detail in section 5.2, Skin Friction Testing.

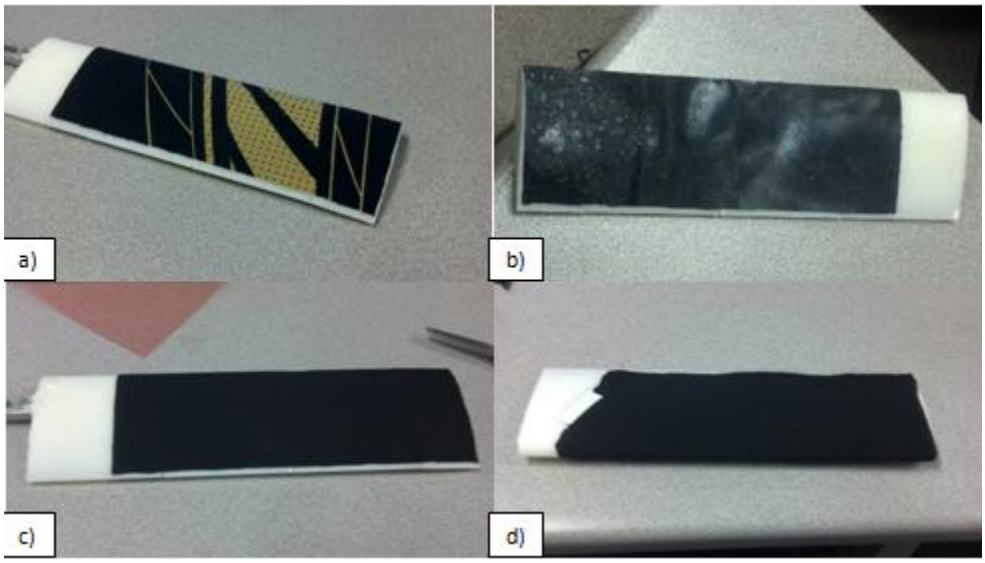

Figure 25. The finished airfoils that have been coated with the suits. (Suit shown: a. TYR AP12, b. Aerosuit, c. Speedo LZR, d. A3 Stealth).

After the airfoil had been covered in the suit, it was inserted into the water channel and screwed into the dynamometer. The water channel was filed to a constant height for all tests, which can clearly be seen in Figure 26. Also shown in Figure 26 is the airfoil connected to the dynamometer (no suit is covering the airfoil in this instance).

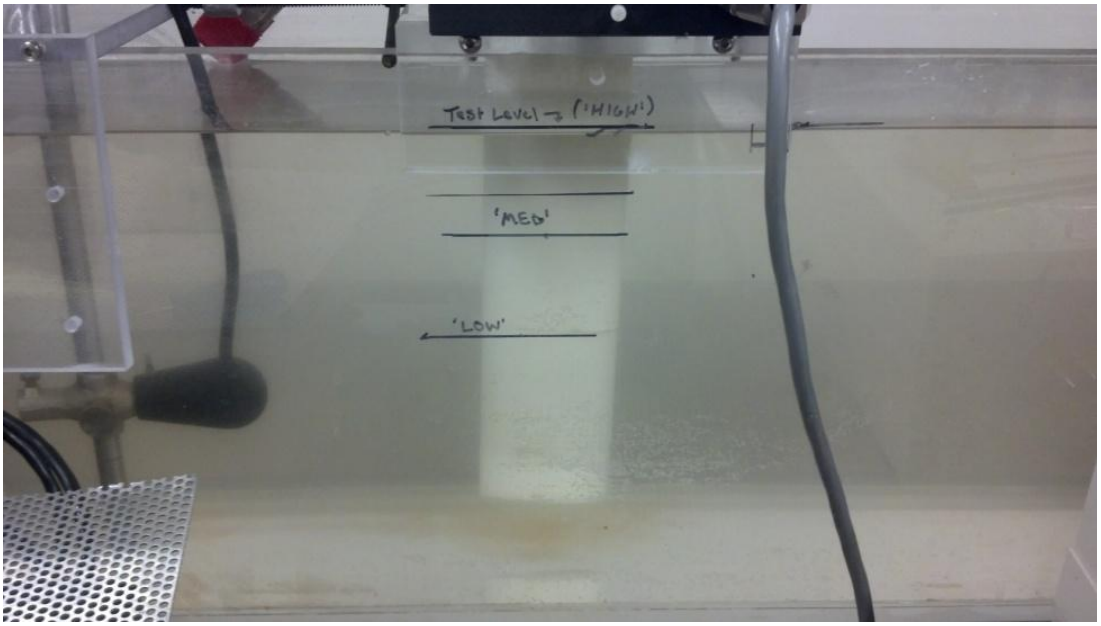

Figure 29. The filled test section of the water channel with the airfoil inside of it and connected to the dynamometer. This setup was used for drag testing. Water was held at this constant level.

After the airfoil had been inserted into the channel, pumps one and three were turned on and the flow was allowed to stabilize for one minute. After this stabilization period, voltage readings were taken using an MCDAQ USB-2408 data acquisition device and Tracer DAQ Pro software for eight minutes at a rate of 6 Hz. Voltage readings were inserted into Microsoft Excel and the average and standard deviation were taken. The average voltage was converted to a mass using the calibration equation in Figure 11. This was then used to calculate the drag force on the airfoil. Each airfoil's drag coefficient was then calculated. An uncertainty analysis was performed on both the force and the drag. A discussion of the results for contact angle and skin friction tests, along with summary data tables, is located in the Results section, which follows.

Chapter 5: Results

The results obtained using the aforementioned procedures are summarized below in Tables 6, 7 and 8 and Figures 30 and 31, with several important aspects of the data highlighted. Appendix C shows pictures of the 2 μL drop contact angle tests as well as the Aerosuit in action.

5.1 Contact Angle Testing

Table 6 shows the summary of the average contact angles for each material when a 2 μL drop was used for testing. Raw data for this data can be found in Appendix D.

Table 6. Average contact angle with uncertainty (based off of statistical variation) for each of the different materials that were tested.

Material on Slide	Average Contact Angle	Uncertainty
75% MTMS Aerogel	147°	±4°
50% MTMS Aerogel	143°	±3°
TYR AP12	139°	±3°
Speedo LZR Elite	143°	±4°
A3 Stealth	135°	±4°

The average contact angle was greater than 130 degrees for all of the different materials, proving that all are superhydrophobic. The aerogels and the Speedo LZR Elite had the highest contact angle measurements. Uncertainty numbers are solely derived from the standard deviation of the 30 readings, and are equal to one standard deviation.

5.2 Skin Friction Testing

Table 7 shows the different materials and the average voltage and standard deviation that was obtained from the ten minute dynamometer tests, as well as the percent standard deviation and flow velocity for the tests.

Table 7. Average voltage and standard deviation for the 10 minute dynamometer tests.

Material	Avg Voltage (V)	Standard Dev Voltage (V)	% Std. Dev	Vel (m/s)
Speedo LZR	1.13	0.13	11.20	0.58
A3 Stealth	1.16	0.12	10.48	0.58
TYR AP12	1.15	0.10	8.71	0.58
50% MTMS Aerosuit	1.12	0.11	10.17	0.58
75% MTMS Aerosuit	1.09	0.11	10.40	0.58
Plain Airfoil	0.92	0.08	8.27	0.58

Table 8 shows the drag force and drag coefficient that was calculated for each of the different materials. Uncertainties are also shown. A propagation of uncertainty was performed to find these values. For more information, see section 5.7, Uncertainty. Testing was performed at a flow velocity of 0.58 m/s for all tests. All other velocities (pump alignments) resulted in flows that were too unstable to be tested at. This equates to a Reynolds Number of 46,400 for all tests. Drag coefficients were calculated using Equation 2.

$$C_D = \frac{F_D}{\frac{1}{2}\rho V^2 A} \qquad (2)$$

Table 8. The drag force and drag coefficient that was obtained from each of the 10 minute dynamometer tests. Uncertainties are also shown.

Material	Equivalent Mass (g)	Drag Force (N)	±	%	Drag Coefficient	±	%
Speedo LZR	15.75	0.1545	0.0181	11.71	0.0387	0.0046	11.83
A3 Stealth	16.30	0.1599	0.0175	10.95	0.0400	0.0044	11.07
TYR AP12	16.10	0.1580	0.0144	9.10	0.0395	0.0037	9.25
50% MTMS Aerosuit	15.64	0.1534	0.0163	10.64	0.0384	0.0041	10.78
75% MTMS Aerosuit	15.23	0.1494	0.0163	10.89	0.0374	0.0041	11.04
Plain Airfoil	12.79	0.1255	0.0110	8.74	0.0438	0.0039	8.99

For the drag coefficient calculation, F_D is the drag force measured by the dynamometer in Newtons, ρ is the density of the water in the test section, in kg/m^3, V is the velocity of the water running over the airfoil in m/s, and A is the planform area of the section of the airfoil that was submerged during the test, in m^2. The planform area value for the uncoated airfoil is 0.017 m^3, which was calculated by multiplying the length times the height of the plain airfoil. The surface area for the covered airfoils was assumed at a constant value of 0.019 m^3, which was calculated by comparing the additional width of the cross sections from the addition of the suit coatings.

Figures 30 and 31 show graphically the data that is represented in Table 8, with error bars. Figure 30 has drag force data and Figure 31 has drag coefficient data. Values for error bars for Figure 30 are shown in the 4th column in Table 8. Values for error bars for Figure 31 are shown in the 7th column in Table 8. Both sets of error bars were calculated during the propagation of uncertainty (see section 5.6, Uncertainty).

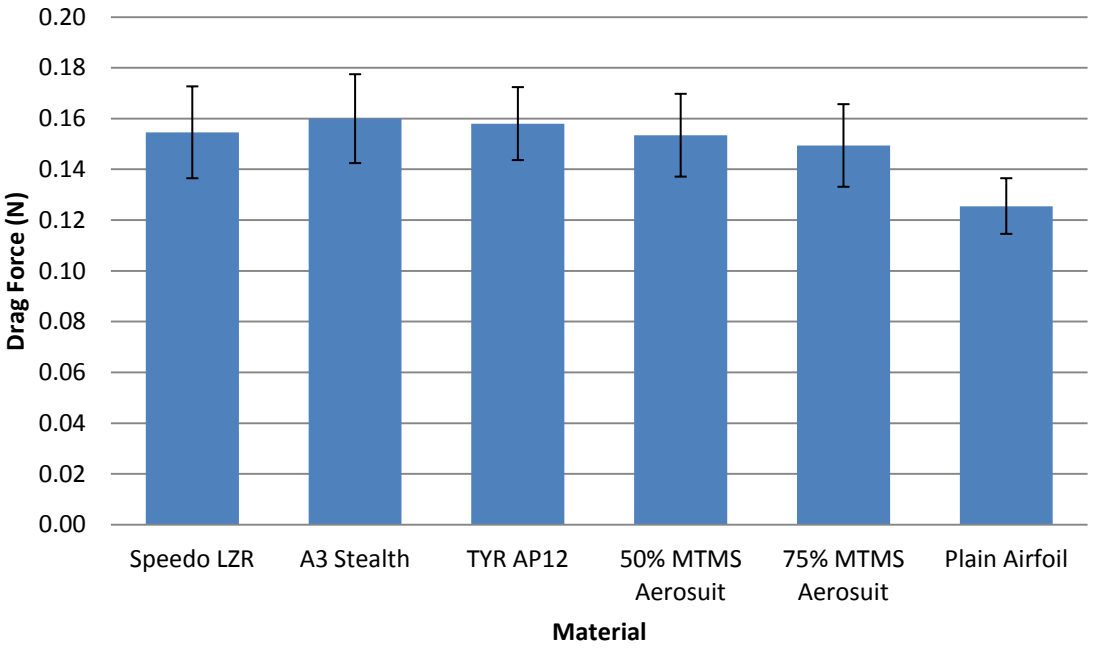

Figure 30. Drag force readings for the materials represented graphically. Error bars are shown.

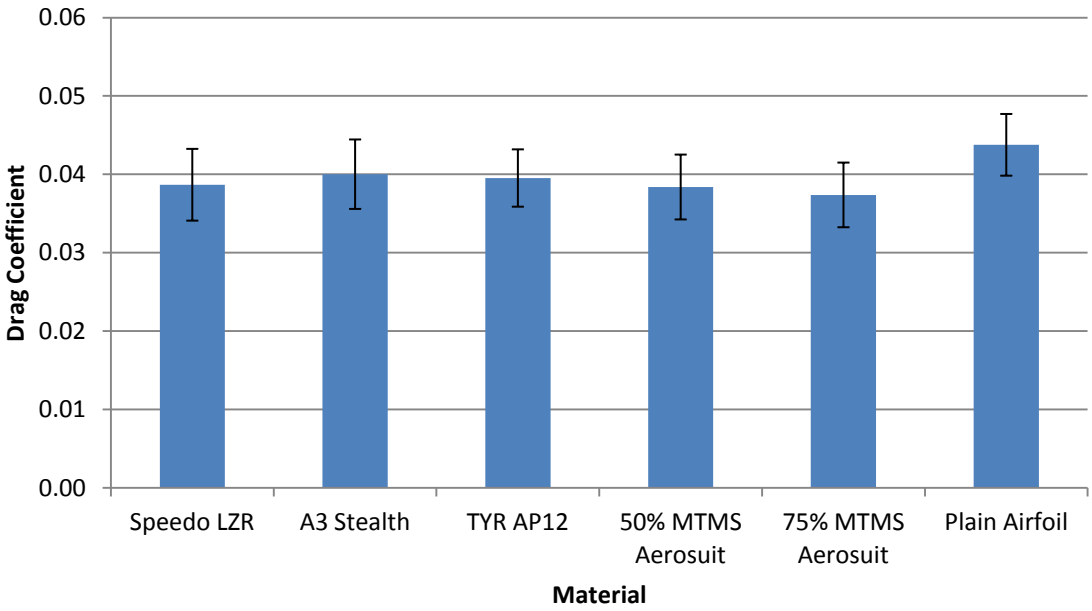

Figure 31. Drag coefficient readings for the materials represented graphically. Error bars are shown.

The data in Table 8 shows that not only did the two Aerosuits perform comparably to the technical swimsuits that were tested, but outperformed all of them. When comparing the data in Table 6 with Table 8 there appears to be a direct correlation between the contact angle of the materials and the drag coefficient of the materials. The Speedo LZR and the 50% MTMS had nearly identical drag readings and contact angles. The 75% MTMS performed the best in both tests. When ranking the other materials in terms of highest contact angle and lowest drag coefficient, the rankings look identical. The 50% MTMS aerogel and the Speedo LZR had the second highest contact angle and the second lowest drag coefficient, the TYR AP12 had the third highest contact angle and the third lowest drag coefficient, and the A3 Stealth had the lowest contact angle and highest drag coefficient.

One thing to note when viewing this data is that during testing neither the bottom, nor the 'tail' end of the airfoil was covered with suits. Because of this, the drag coefficients

might actually be lower than what was calculated here. With this in mind, the data shown here proves the plausibility of a technical suit that utilizes the hydrophobic properties of aerogels in order to reduce drag.

It is important to note that although the plain airfoil that was tested required less force than all of the suits, the drag coefficient that is calculated from this force measurement is larger than that of all of the suits. The reason for the lower magnitude in drag force is due to the size of each of the test items. When the airfoil was covered in each of the suits (as well as the double sided tape that was required to keep the suit attached to the airfoil) the surface area of the airfoil increased significantly. This factor is accounted for when the drag coefficient is calculated. The plain airfoil was calculated to have the highest drag coefficient despite creating the least drag force.

A value for the drag coefficient for this type of airfoil (NACA 0012) at a Reynolds Number of 40,000 has been reported at 0.025 (Laitone, 1997). This is higher than the value that was calculated for the plain airfoil in this test. This is most likely due to the roughness of the airfoil that was used. See section 5.3, Comparison to Predicted Performance for more information.

5.3 Comparison to Predicted Performance

Prior to the tests, a calculation was performed in Matlab to determine what the expected drag readings should be for the plain base airfoil. It was found, prior to testing, the airfoil should exhibit a drag force of 0.0424 Newtons, which is equivalent to 0.0043 kg. The Matlab code used to generate this result can be found in Appendix E. When comparing these calculations to the experimentally obtained numbers there is a large difference

between both the drag force and mass for both cases. Experimentally it was found that the drag force on the airfoil was 0.1255 Newtons, which is equivalent to 0.0128 kg. This result is not surprising when the drag coefficient used in the calculation (0.025, which was an assumed value based on the geometry of the airfoil) is compared to the experimentally calculated drag coefficient (0.044). The drag coefficients vary. This difference is what caused the differences in force. This result shows that, although the calibration of the dynamometer was performed well, something about the geometry of the airfoils is driving up the drag force. This is most likely the roughness that is present on all faces of the airfoil. Because the airfoil was prepared in a 3D rapid prototyping machine, there was visible surface roughness present (due to the layering method used to create it). This most likely increased the drag from the water flowing over it. The magnitude of the drag coefficient that was calculated for the plain airfoil is appropriate, which means that the data presented is also the correct order of magnitude.

5.4 Plausibility of Experiment in Relation to Swimming

It has been proven that the Aerosuits performed at least comparably to the commercially available technical suits in the outlined tests. It is now possible to consider the relatability of these tests to swimming. The most effective way of doing this is by considering the Reynolds Numbers of the situations in which the suits are typically used and comparing these values to the Reynolds number of the dynamometer tests.

It is possible to perform a back of the envelope calculation for the Reynolds Number of each of the individual events that are performed at international swimming competitions (like the Olympics). In order to do this, a few assumptions must be made:

1. Swimmers travel at a constant speed during their races
2. The temperature of the water in which each swim is completed is constant
3. The temperature of the water in each pool is 26° C
4. The length of the suit on the legs of a male swimmer is 45 cm (0.45 m)

In order to calculate the Reynolds Number, which is a ratio of the inertial forces acting on an object to the surface forces acting on that object, Equation 3 used.

$$Re = \frac{\rho V L}{\mu} \quad (3)$$

Where ρ is the density of the fluid, V is the velocity of the fluid flow (or item moving through the fluid), L is the characteristic length of the item, and μ is the dynamic viscosity of the fluid.

Velocities used for each calculation were obtained by simply dividing the distance of each event by the world record time for each event. Each event, world record time, and calculated velocity can be found in Table 9 (12).

Table 9: Each event swum at the Olympics with world records and calculated average velocities.

Event	Distance (m)	World Record (min)	World Record (sec)	Velocity (m/s)
50 Free	50	20.91	20.91	2.39
100 Free	100	46.91	46.91	2.13
200 Free	200	1:42.00	102.00	1.96
400 Free	400	3:40.07	220.07	1.82
800 Free	800	7:32.12	452.12	1.77
1500 Free	1500	14:31.02	871.02	1.72
100 Fly	100	49.82	49.82	2.01
200 Fly	200	1:51.51	111.51	1.79
100 Back	100	51.94	51.94	1.93
200 Back	200	1:51.92	111.92	1.79
100 Breast	100	58.46	58.46	1.71
200 Breast	200	2:07.01	127.01	1.57
200 IM	200	1:54.00	114.00	1.75
400 IM	400	4:03.84	243.84	1.64

Using the velocities calculated in Table 9, a characteristic length of 45 cm, a density of 996.8 kg/m^3, and a dynamic viscosity of 0.000871 Pa-s, it is possible to calculate the Reynolds Number of each case. Calculated Reynolds Numbers can be found in Table 10.

Table 10. Reynolds Number calculated for each event.

Event	Velocity (m/s)	Reynolds Number
50 Free	2.39	1,231,454
100 Free	2.13	1,097,835
200 Free	1.96	1,009,793
400 Free	1.82	936,055
800 Free	1.77	911,252
1500 Free	1.72	886,881
100 Fly	2.01	1,033,710
200 Fly	1.79	923,674
100 Back	1.93	991,518
200 Back	1.79	920,290
100 Breast	1.71	880,934
200 Breast	1.57	810,951
200 IM	1.75	903,499
400 IM	1.64	844,807

It was found that the highest Reynolds Number happened during the 50 meter freestyle (over 1.2 million) and the lowest Reynolds Number happened during the 200 breaststroke. This is expected, as they have the highest and lowest velocities, respectively. The Reynolds Number for the testing of the airfoils covered in suits was calculated (assuming a temperature of 20° C and a characteristic length of .06985 m, the width of the airfoil) to be 40,400. This is significantly lower than any of the calculated world record Reynolds Numbers.

5.5 Suit Trial

Upon the completion of the coating of the 50% MTMS Aerosuit, I performed a test run of the prototype swimsuit. I put on the suit and did various activities that simulated the type of action that the suit would see in a race setting. The suit had a similar feel to that of a typical racing suit (ask any swimmer-they can feel the difference between racing suits and practice suits). It felt easier to 'slip' through the water when the suit was worn. Photographs were taken underwater of the suit in action. Photographs of the suit can be seen in Appendix C. When viewing these photographs, one can see that there is a visible air bubble around the suit, which is ideal. This bubble serves as a means to 'violate' the no-slip condition, which causes a significant decrease in viscous drag.

5.6 Discussion of Assumptions and Results

The assumption of pool water being 26° C for the times located in Table 9 comes from the FINA Bureau. According to the group, the optimal pool temperature for racing is 26° C (FINA Bureau, 2011). The assumption of suit length is based upon observation. The typical male Olympic Swimmer is around 6 feet 4 inches tall (much larger than the average human). Most individuals this size will wear a size 30 bathing suit (based upon the circumference of the waist). The length of a size 30 bathing suit is approximately 43 cm. Allowing for the stretching that occurs when one of these racing suits is worn, this number is adjusted to 45 cm.

The assumption of constant speed is not very accurate, as the speed of a swimmer will vary greatly throughout a race. When swimmers push off of turns in what is known as 'streamline position' (with their arms above their head, squeezed together in an attempt to

create a long, slender shape), they will have a velocity that is significantly higher than when they are swimming in the middle of the pool. Also, fatigue sets in at the end of a race, and swimmers typically slow down as compared to their starting pace. This fatigue effect is most apparent in the middle-distance races, around 200 meters. In longer races swimmers tend to get into a 'rhythm' with their swimming and hold pace the entire time. In shorter races swimmers will not fatigue as much as they are not required to exert for as long of a time.

When considering the Reynolds Numbers, it is important to consider that the calculations are for world record times. The speed that these swimmers are able to propel themselves forward is significantly higher than the average swimmer. For some little children who are just learning to swim fast, a speed of 0.58 m/s is actually significantly faster than they could move through the water. This is about the max speed of the average male high school swimmer. The Reynolds number of this same swimmer would be much higher, however, as their characteristic length will be larger than that of the airfoil. In order to obtain Reynolds Numbers on the same order as those of the world record swimmers, with the airfoil that was used for testing in this experiment, necessary velocities would range from 10.1 to 15.4 m/s. Table 11 shows the full breakdown of speeds necessary to test at similar Reynolds Numbers.

If future testing were to be performed, the velocities shown in Table 11 would only be needed with an airfoil that was the same size as the one used for testing in this experiment. It would be wise to both increase the size of the airfoil (or whatever object was being covered in suits) and increase the flow velocity. Increasing the size of the test object would result in lower flow velocity requirements, ultimately making the goal Reynolds Numbers more obtainable.

Table 11. Flow velocities needed in order to run tests at similar Reynolds Numbers to world record swimmers.

Event	Necessary Velocity (m/s)
50 Free	15.41
100 Free	13.73
200 Free	12.63
400 Free	11.71
800 Free	11.40
1500 Free	11.09
100 Fly	12.93
200 Fly	11.55
100 Back	12.40
200 Back	11.51
100 Breast	11.02
200 Breast	10.14
200 IM	11.30
400 IM	10.57

Although the Reynolds Numbers that the tests were performed at are significantly lower than those of world record swimmers, the results from the dynamometer drag readings are still a good base for future testing, and prove that a suit that is coated with aerogels is a feasible option for a technical swimsuit. If possible, future testing might involve trying to prove that the Aerosuit performs better at all Reynolds Numbers.

5.7 Uncertainty

A full uncertainty analysis for the drag force values and drag coefficient values can be seen in Appendix F. Uncertainties that were obtained have a reasonable magnitude, but do provide a slight problem when trying to prove the data is certain. Because all of the calculated drag coefficients are so similar in magnitude, even with this small level of uncertainty (less than 13.5% at the highest) the results cannot be considered conclusive. This, however, does not take away from the fact that a technical swimsuit created with

aerogels that will perform comparably to the top technical suits available today is plausible. In order to make these numbers more concrete, their uncertainties will have to be lowered. Potential modifications that may be performed on the the water channel in order to increase the uniformity in the flow will be discussed in the Summary and Future Work section, which follows.

Chapter 6: Summary and Future Work

6.1 Summary

In this work I have completed the build of the water channel at Union College and successfully modified the design in order to provide a temporary fix for uncertainty values that are derived from variations in the flow (to an acceptable level). I have successfully created a prototype swimsuit that is covered with aerogel material, and tested it out firsthand inside of the pool. I have also done testing on different technical swimsuits and aerogels and compared the two, proving the plausibility of a suit that relies on the hydrophobic properties of silica aerogels to decrease the effects of viscous drag on a swimmer.

6.2 Future Work

With respect to the water channel, the two obvious steps that need to be taken in the future involve decreasing the level of uncertainty in the dynamometer readings, and providing a permanent fix to the issues that were experienced in the water channel. If someone chooses to continue on with the research that I have started, these should be the starting points for their project. Further work would also include measuring drag forces at much higher Reynolds Numbers (see section 5.6). An entire senior project can be devoted to increasing the uniformity of the flow inside of the water channel. Appendix G shows a complete list of suggestions for improvements that can be made to the water channel.

Acknowledgements

I would like to thank Rob Wagner for providing an excellent start to the water channel, and for help troubleshooting issues that arose during its assembly. Paul Tompkins has been supremely helpful in designing parts and discussing problems that have come up at all points in the project, as well as aid in moving the water channel. Stan Gorski has been a great asset when it came to devising a fabricating test piece to be inserted into the channel. Special thanks goes out to all of the Fluids I students who allowed me to take over the wind tunnel lab in the basement of Science and Engineering while they were down there performing tests for the labs. Finally, I would like to thank Professor Anne Anderson for her continual support and encouragement on this project, as well as her unending technical knowledge and Advice.

References

1. Anderson, Ann M.; Carroll, Mary K.; Green, Emily C.; Melville, Jason T.; Bono, Michael S., 2009 "Hydrophobic silica aerogels prepared via rapid supercritical extraction," Polymer Preprints, 52(1), pp. 32.
2. "Arena Powerskin Carbon Pro Jammer." Chain Reaction Cycles. *Image*. Nov 4th, 2012. <http://chainreactioncycles.com>
3. Carrol, Mary K.; Anderson, Ann M., 2011 "Use of a rapid supercritical extraction method to prepare aerogels from various precursor chemistries," Journal of Sol-Gel Science and Technology, 53(2), pp. 199-207.
4. FINA Bureau., 2011 "FINA Requirements for swimwear approval," Lausanne, Switzerland.
5. Gou, S.; Mossman, M.; Whitehead, L., 2012 "Transparent superhydrophobic surfaces for applications of controlled reflectance," Journal of Applied Optics, 51, pp. 1645-1653.
6. Laitone, E. V., 1997, "Wind Tunnel Tests of Wings at Reynolds Numbers Below 70,000," Experiments in Fluids, 23, pp. 405-409.
7. "Plasma Cleaning Figure." Harrick Plasma Corporation. *Image*. Nov 15th, 2012. <http://harrickplasma.com>
8. Rodriguez, Justin E.; Anderson, Ann M.; Carroll, Mary K., 2012 "Drag Reduction Characteristics of Surfaces Coated with Super-Hydrophobic and Hydrophilic Silica Aerogel Material," Manuscript submitted to Journal of Colloids and Interface Science.
9. "Speedo FS3 Elite Jammer." All American Swim. *Image.* Nov 4th, 2012. <http://allamericanswim.com>
10. Truesdall, Richard; Mammoli, Andrea; Vorobeiff, Peter; Swol, Frank van; Brinkler, C. Jeffrey., 2006 "Drag Reduction on a Patterned Superhydrophobic Surface," Physical Review Letters, 97(4), pp. 100-104.
11. "TYR AP12 Compression Speed Short." Pure Blue Swim. *Image*. Nov 4th, 2012. <http://pureblueswim.com>

12. Wagner, Robert J., 2012 “Redesign and Assembly of an Open Surface Water Channel,” Schenectady, New York, United States.
13. “World Records in Swimming.” Wikipedia. March 14th 2013. <http://wikipedia.com>

Appendix A: Wagner's Report

(Begins on next page)

Appendix B: Reynolds Number Calculation

Reynolds Number is a dimensionless flow parameter equivalent to the ratio of surface forces to body forces and can be calculated using:

$$Re = \frac{\rho V L}{\mu}$$

Where:

ρ is the density of the fluid

V is the velocity of the flow

L is a characteristic linear dimension associated with the flow

μ is the dynamic viscosity of the fluid

MATLAB Input:

```
% November 4th, 2012 at 9:00 p.m.
%Given that the max. flow speed measured was 0.74 m/s, when the temp is
%assumed to be 70 F, the max attainable Re can be calculated (for the
%current water channel design).

clear
clc

v = 0.74; % m/s

%STRAIGHT!

L = 12; % in
L = L*.0254 % m
dens = 998.2; % kg/m^3
visc = 1.002E-3; % lb*s/ft^2
Re_max = dens*v*L/visc
```

MATLAB Output:

```
Re_max =  2.2470e+005
```

Appendix C: Contact Angle and Suit Pictures

Below each photograph is a caption explaining the picture.

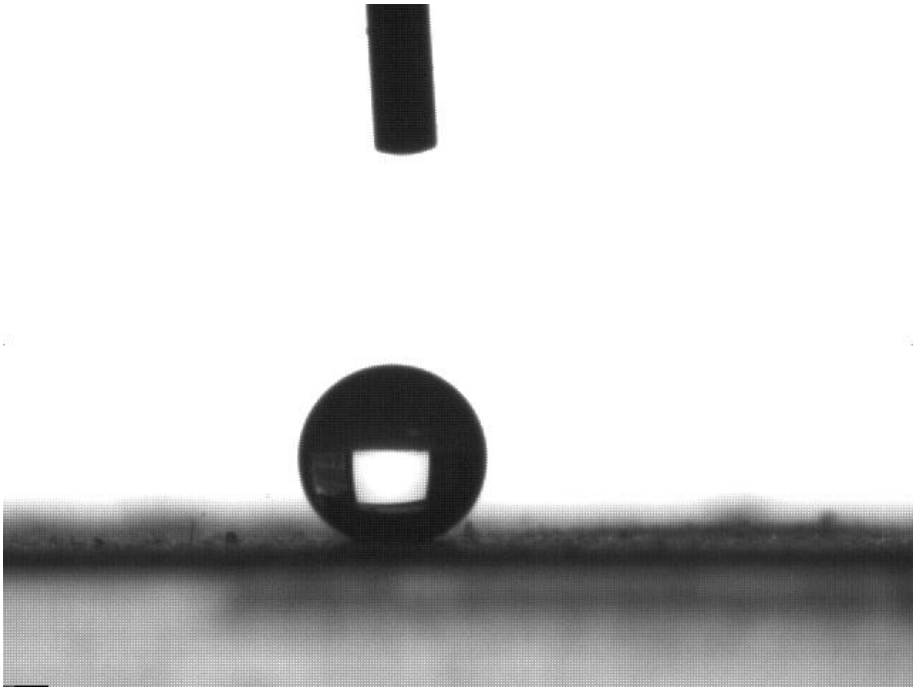

Photograph of a 2 µL drop of water on ground up 75% MTMS aerogels. The average contact angle of this material was 147°, the highest recorded value for any of the items that were tested.

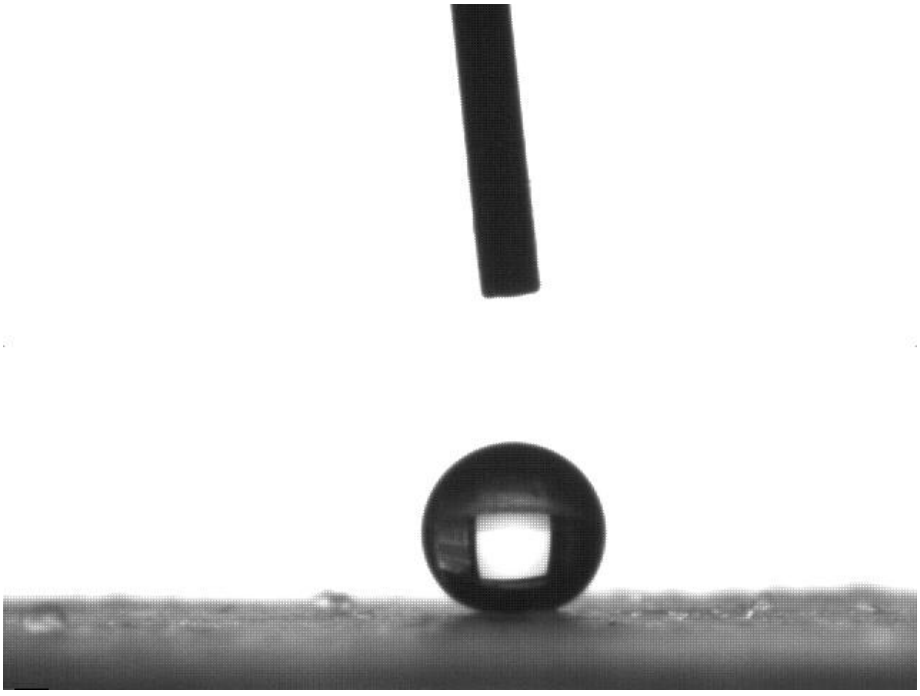

Photograph of a 2 µL drop of water on ground up 50% MTMS aerogels. The average contact angle of this material was 143°, the same as the Speedo LZR racing suit.

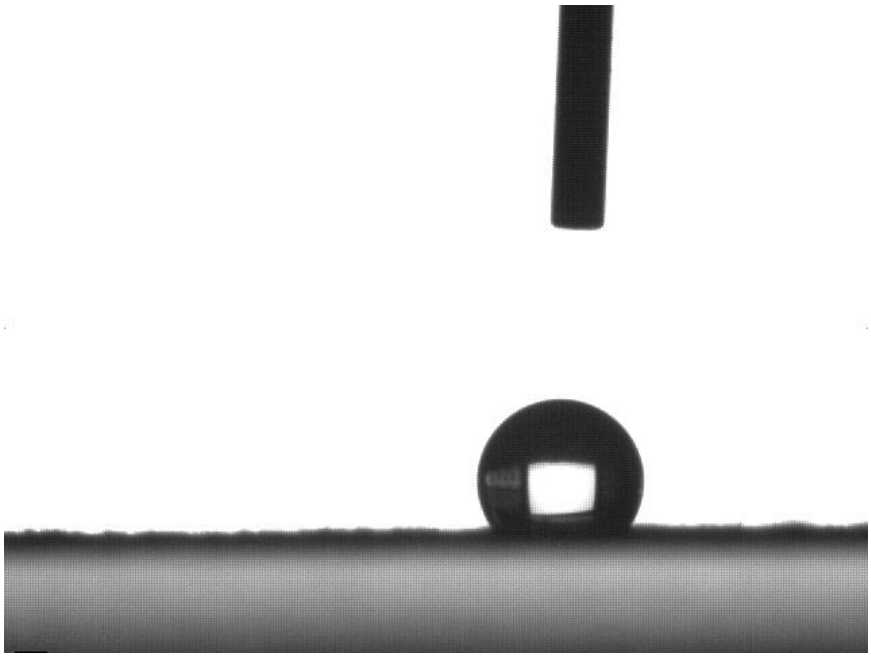

Photograph of a 2 µL drop of water on a slide covered with the A3 Stealth racing suit. The average contact angle of this material was 135°. Note the significantly larger amount of contact with the surface than the 50% and 75% MTMS photo (above)

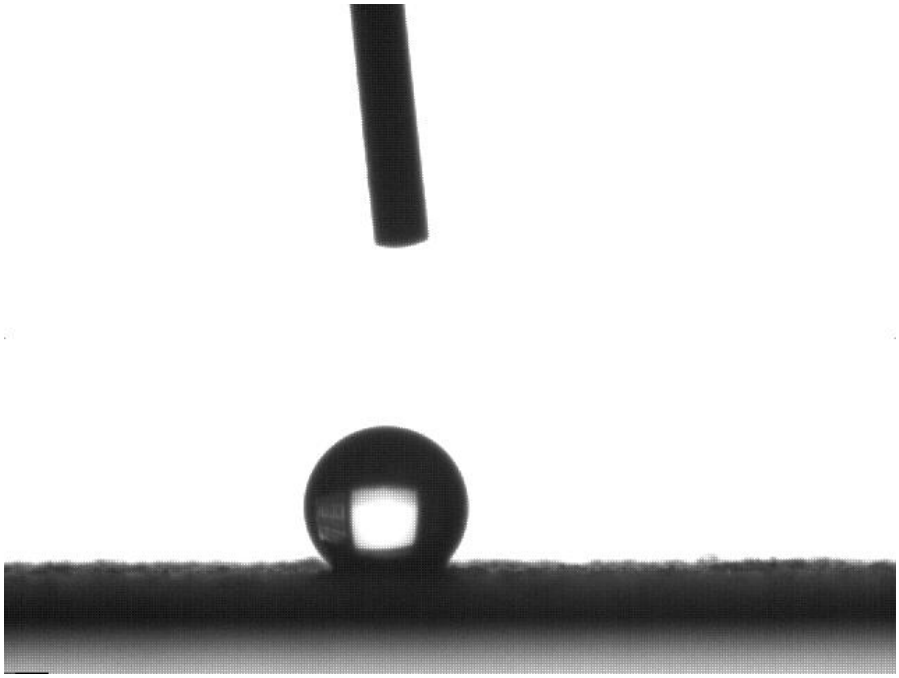

Photograph of a 2 µL drop of water on a slide covered with the Speedo LZR racing suit. The average contact angle of this material was 143°. Note the similarity in appearance to the 50% MTMS photo.

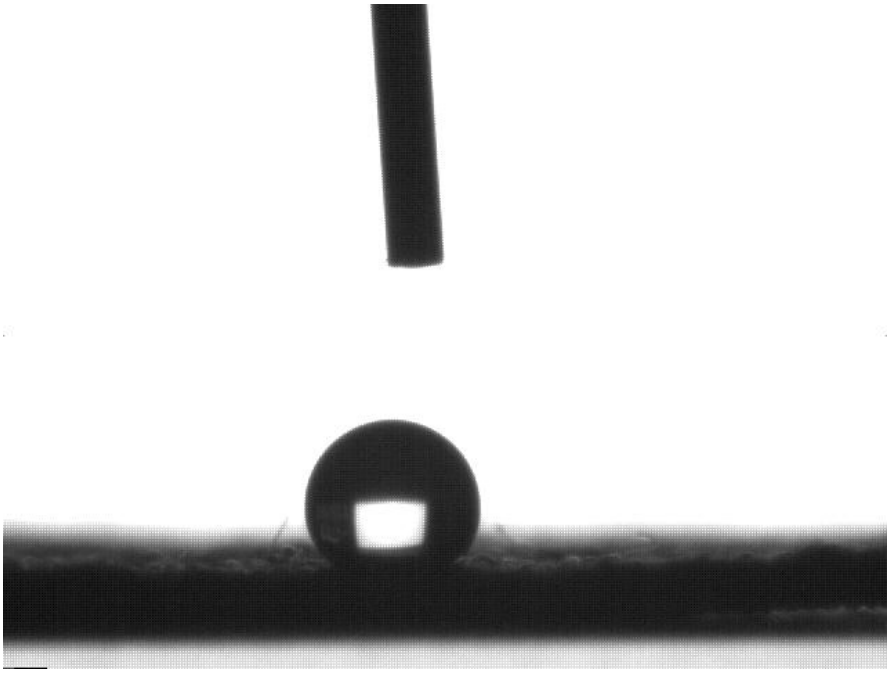

Photograph of a 2 µL drop of water on the surface of a slide covered with the TYR AP12 racing suit. The average contact angle of this material was 139°. This was one of the lowest contact angles measured for any of the suits.

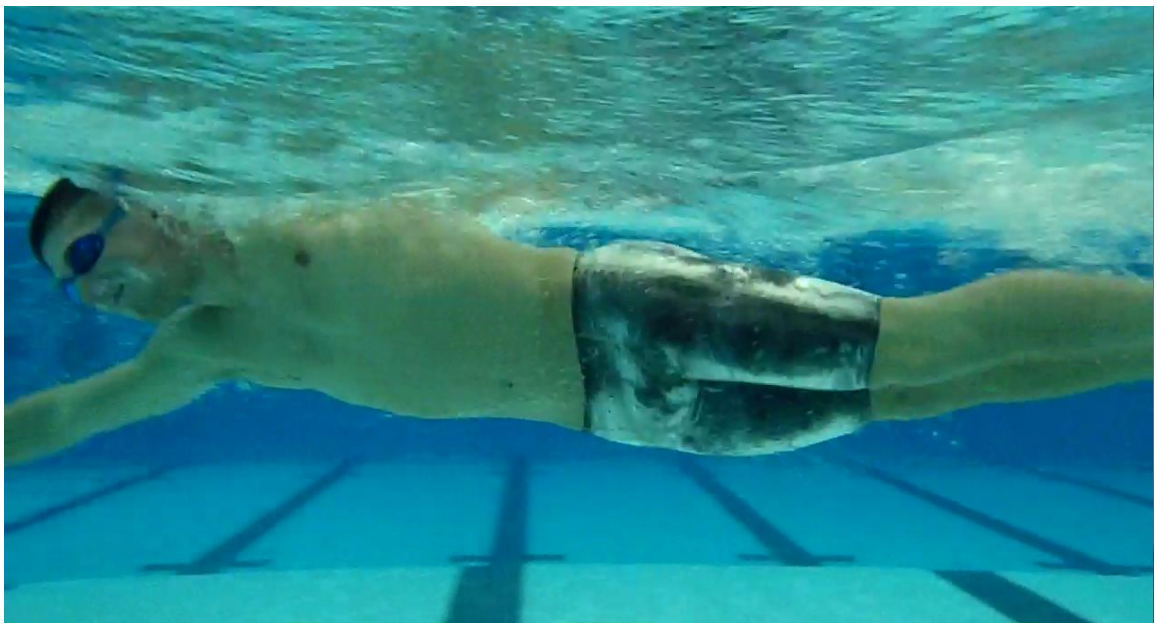

Photograph of the 50% MTMS Aerosuit in action from the side. Note the shiny air bubble that has enveloped the suit entirely, reducing the amount of viscous drag from the water.

Photograph of the bottom view of the 50% MTMS Aerosuit in use. The air bubble surrounding the suit is very visible from this angle. Bubbles created by the swimmer have similar reflective properties as the bubble enveloping the suit.

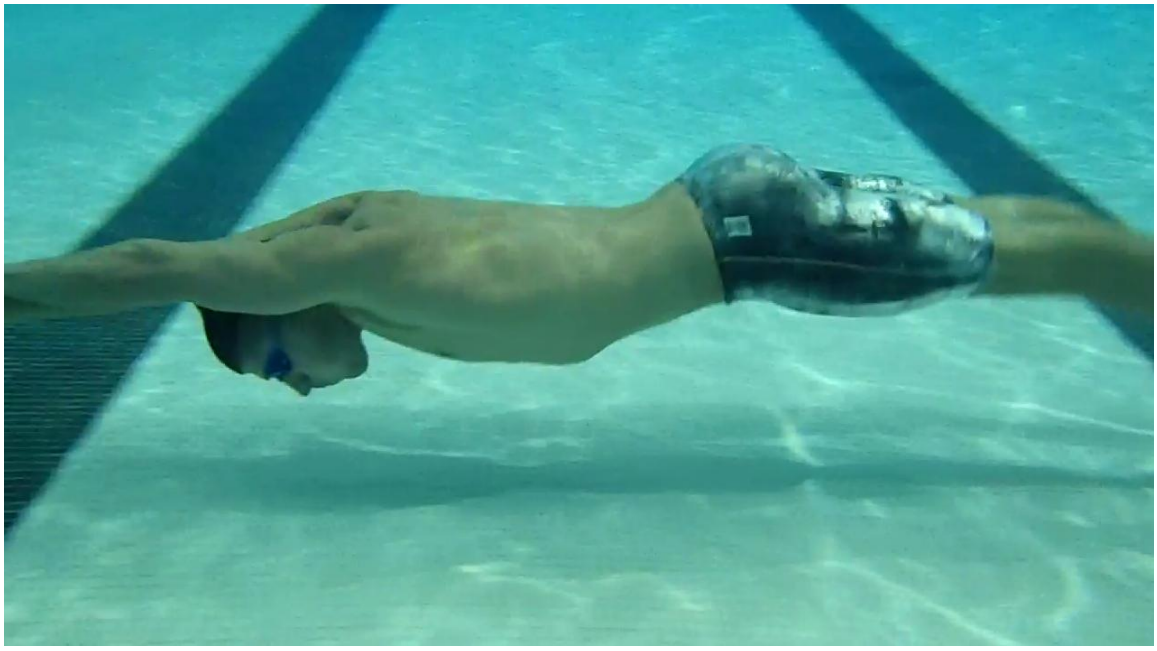

Photograph of the suit while kicking underwater. Even at lower depths the bubble around the suit is still present.

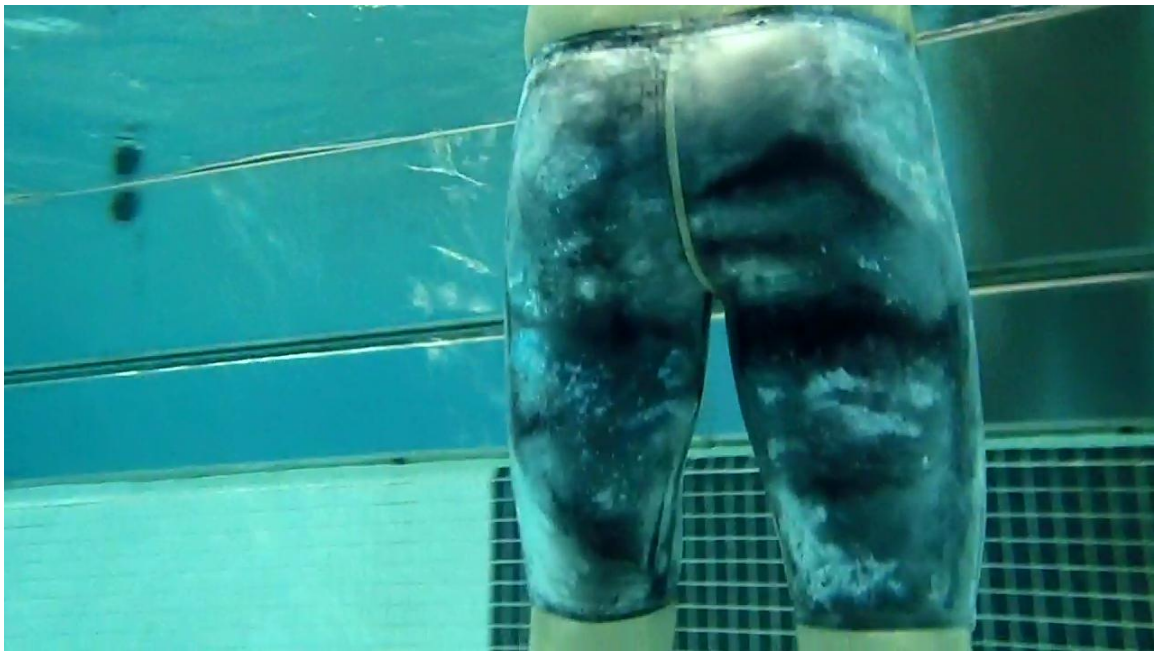

Photograph of the suit while standing, after extended period of time spent in water. Even after a long time the bubble around the suit is still present.

Appendix D: Contact Angle Raw Data

Table 1 shows the raw data for the contact angle measurements for each material. The average value and standard deviation are calculated from this data.

Table 1. Raw data for the contact angles for the different materials.

Trial	75% MTMS Aerogel	50% MTMS Aerogel	TYR AP12	Speedo LZR Elite	A3 Stealth
1	148.8	143.6	137.2	136.1	133.7
2	151.4	149.0	138.3	142.5	129.6
3	145.1	144.3	138.5	151.1	140.5
4	149.2	144.6	142.7	136.4	132.4
5	148.5	140.1	139.4	146.6	138.4
6	146.6	141.2	138.3	143.7	129.7
7	147.9	145.8	138.6	139.9	137.9
8	145.0	136.1	138.5	143.3	137.2
9	147.7	149.4	144.8	151.2	143.0
10	148.5	140.7	139.9	137.3	140.9
11	153.9	139.1	137.4	151.9	128.9
12	149.0	142.9	140.2	138.0	130.9
13	153.7	146.4	144.7	139.8	131.8
14	145.6	140.5	137.7	143.0	134.3
15	147.9	146.7	141.8	139.5	129.1
16	143.0	140.6	141.6	142.2	133.5
17	141.7	142.7	137.3	138.5	139.6
18	155.1	138.7	136.4	142.2	134.5
19	141.4	140.1	133.6	139.4	132.2
20	142.4	145.3	137.1	140.3	134.6
21	142.1	140.1	134.2	152.2	131.3
22	146.0	142.1	137.2	141.5	132.8
23	143.5	139.1	140.1	149.5	141.2
24	145.8	142.9	140.5	150.4	139.0
25	145.4	143.5	140.9	139.0	140.7
26	151.4	141.7	142.0	143.6	131.0
27	141.4	146.1	144.4	146.4	133.8
28	145.4	146.3	141.0	137.3	132.4
29	152.0	141.3	134.3	144.4	133.0
30	153.3	146.3	135.1	143.8	134.2
Avg	**147**	**143**	**139**	**143**	**135**
Std Dev	**4**	**3**	**3**	**4**	**4**

Appendix E: Expected Drag Force on Plain Airfoil

Drag Force is the amount of force that is created by the fluid flowing over an object and can be calculated using the following (modified version of Equation 2):

$$F_D = \frac{\rho v^2 C_D}{2}$$

Where:

ρ is the density of the fluid

v is the velocity of the flow

A is the surface area of the item inside the flow

C_D is the drag coefficient of the item inside the flow

MATLAB INPUT

```
% March 14th, 2012 at 1:30 p.m.
% Given that the flow speed drag readings were taken at was 0.58 m/s, the
% surface area of the airfoil is 0.010104 m^2, the density of water
% is 998.2 kg/m^3 at 70 C, and the drag coefficient for the airfoil used
% is 0.075, the expected force can be calculated

rho = 998.2; %kg/m^3
v = 0.58; %m/s
Cd = 0.025;
A = .010104; %m^2

F_d = 0.5*rho*v^2*Cd*A %N

mass = F_d/9.81 %kg
```

MATLAB Output:

```
F_d =0.0424

mass=0.0043
```

Appendix F: Uncertainty Analysis for Drag Calculations

To demonstrate the method used to find the uncertainty in each calculation, a dummy calculation is performed below for the uncertainty in the drag force and drag coefficient of the Speedo LZR swimsuit. Uncertainties in the other materials are performed using the same process.

In order to find the uncertainty in the force measurement it was first necessary to calculate the uncertainty in the conversion from a voltage to a mass. To do this, a propagation of uncertainty was performed on Equation 1. Equation 3 represents the partial derivative of Equation 1 with respect to the Voltage variable.

$$\frac{\partial M}{\partial V} = 14.64 \tag{4}$$

Noting that the total uncertainty in one calculation of mass is equal to the root sum square of the uncertainty values of the voltage squared multiplied times its partial derivative squared:

$$\delta M = \sqrt{(\frac{\partial M}{\partial V})^2 (\delta V)^2} \tag{5}$$

Contributions to the uncertainty in the voltage come only from the standard deviation of the readings. The uncertainty in the voltage for the Speedo LZR is equal to:

$$\delta V = 0.1260 \text{ V}$$

Plugging these into Equation 4:

$$\delta M = \sqrt{(14.64)^2 (0.1260)^2} = 1.8444 \text{ grams}$$

Using this result it is possible to calculate the percent uncertainty in the voltage measurement such that:

$$\% = \left(\frac{\delta M}{M}\right) * 100 = \frac{1.8444}{15.75} * 100 = 11.20\%$$

The next step in finding the uncertainty in the force measurement is performing a propagation of uncertainty on Equation 5, Newton's Second Law:

$$F_D = Mg \tag{6}$$

Assuming that the acceleration due to velocity is constant, the only variable in this equation is the mass value (which was calculated using the calibration equation). Taking the partial derivative of Equation 5 with respect to this variable results in:

$$\frac{\partial F_D}{\partial M} = g = 9.81$$

Noting that the total uncertainty in one calculation of force is equal to the root sum square of the uncertainty values of the mass multiplied times its partial derivative squared:

$$\delta F_D = \sqrt{(\frac{\partial F_D}{\partial M})^2 (\delta M)^2} \tag{7}$$

Plugging in values into equation 6 and converting to consistent units:

$$\delta F_D = \sqrt{(9.81)^2 (1.8444/1000)^2} = 0.0181 \text{ N}$$

Using this result it is possible to calculate the percent uncertainty in the force calculation such that:

$$\% = \left(\frac{\delta F_D}{F_D}\right) * 100 = \frac{.01545}{0.1545} * 100 = 11.47\%$$

In order to find the uncertainty in the drag coefficient calculations, it is possible to perform a similar procedure. Starting with Equation 2 and performing the partial derivative with respect to each of the variables yields Equations 7 through 10.

$$\frac{\partial C_D}{\partial F_D} = \frac{2}{\rho v^2 A} \tag{8}$$

$$\frac{\partial C_D}{\partial \rho} = \frac{-2F_D}{\rho^2 v^2 A} \tag{9}$$

$$\frac{\partial C_D}{\partial v} = \frac{-4F_D}{\rho v^3 A} \tag{10}$$

$$\frac{\partial C_D}{\partial A} = \frac{-2F_D}{\rho v^2 A^2} \quad (11)$$

Noting that the total uncertainty in one calculation of the drag coefficient is equal to the root sum square of the uncertainty values for each of the variables squared multiplied times its respective partial derivative squared:

$$\delta C_D = \sqrt{(\frac{\partial C_D}{\partial F_D})^2(\delta F_D)^2 + (\frac{\partial C_D}{\partial \rho})^2(\delta \rho)^2 + (\frac{\partial C_D}{\partial v})^2(\delta v)^2 + \left(\frac{\partial C_D}{\partial A}\right)^2 (\delta A)^2}$$

(11)

Noting that the uncertainty in each of the variables:

$\delta F_D = 0.0181$ N

$\delta \rho = 0.05$ kg/m^3

$\delta v = 0.005$ m/s

$\delta A = 0.00005$ m^2

Plugging in values for Equations 7 through 10:

$$\frac{\partial C_D}{\partial F_D} = \frac{2}{\rho v^2 A} = \frac{2}{(998.2)(0.58)^2(0.0238)} = 0.2503$$

$$\frac{\partial C_D}{\partial \rho} = \frac{-2F_D}{\rho^2 v^2 A} = \frac{-2\ (0.1537)}{(998.2)^2(0.58)^2(0.0238)} = 0.00004$$

$$\frac{\partial C_D}{\partial v} = \frac{-4F_D}{\rho v^3 A} = \frac{-4(0.1537)}{(998.2)(0.58)^3(0.0238)} = 0.13$$

$$\frac{\partial C_D}{\partial A} = \frac{-2F_D}{\rho v^2 A^2} = \frac{-2(0.1537)}{(998.2)(0.58)^2(0.0238)^2} = 1.62$$

Plugging all of these values into Equation 11:

$$\delta C_D = \sqrt{(\frac{\partial C_D}{\partial F_D})^2(\delta F_D)^2 + (\frac{\partial C_D}{\partial \rho})^2(\delta \rho)^2 + (\frac{\partial C_D}{\partial v})^2(\delta v)^2 + \left(\frac{\partial C_D}{\partial A}\right)^2 (\delta A)^2}$$

$$= \sqrt{(0.2503)^2(0.0181)^2 + (0.00004)^2(0.05)^2 + (0.13)^2(0.005)^2 + (1.62)^2(0.00005)^2}$$

$$= 0.0046$$

Using this result it is possible to calculate the percent uncertainty in the drag coefficient calculation such that:

$$\% = \left(\frac{\delta C_D}{C_D}\right) * 100 = \frac{.0046}{0.0387} * 100 = 11.83\%$$

Appendix G: Suggestions for Water Channel

Although the water channel performed well for these preliminary tests, there are several changes that need to be made in order for more accurate future testing to occur. Suggested changes are listed below:

- Addition of permanent flow conditioning before the test section in order to increase flow uniformity.
- Patching up of small leaks that are still apparent at the inlet and outlet of the pumps.
- Addition of some sort of water treatment to prevent the appearance of hard water deposits on the walls of the channel.
- Addition of a more accurate flow velocity measurement device.
- Addition of setup that can be used for Particle Image Velocimetry.
- Addition of permanent thermometer to measure the temperature of the water.
- Possible enclosure of the entire 'top' of the water channel (including test section) to allow for increased volumes of water, and faster, more uniform flow.
- Movement of channel to separate room from the wind tunnel.
- Additional dynamometer for the water channel (so that the one from the wind tunnel no longer needs to be borrowed).
- Somehow modifying the channel so that much higher velocity flows can be created.